Isobutanol-Methanol Mixtures from Synthesis Gas

Quarterly Technical Progress Report DOE/PC/94066--T9

Period Covered: 1 October to 30 December 1996

Contractor

University of California-Berkeley
Berkeley, California 94720

Enrique Iglesia - Program Manager

1 March 1997

Prepared for the United States Department of Energy *
Under Contract Number DE-AC22-94PC94066
Contract Period 1 October 1994 - 30 September 1997

DISCLAIMER

Portions of this document may be illegible electronic image products. Images are produced from the best available original document.

TABLE OF CONTENTS

EXECUTIVE SUMMARY

A series of MgO-based Cu catalysts have been prepared by coprecipitating the corresponding metal nitrates with a mixed solution of potassium carbonate and potassium hydroxide. The bulk composition of the catalyst has been measured by atomic absorption (AA) analysis and the Cu dispersion has been determined by N_2O titration at 363 K.

Kinetic studies of ethanol coupling reactions on $Cu_{0.5}Mg_5CeO_x$ and 1.0 wt % K-$Cu_{0.5}Mg_5CeO_x$ catalyst indicates that at similar steady-state acetaldehyde concentrations, the presence of K increases the rates of base-catalyzed aldol coupling reactions to acetone and butyraldehyde. Aldol coupling chain growth reaction rates on 1.2 wt % K-$Cu_{7.5}Mg_5CeO_x$ are higher than on 1.0 wt % K-$Cu_{0.5}Mg_5CeO_x$ even though basic site densities are similar on both samples, suggesting that Cu metal sites are also involved in rate-determining steps required for condensation reactions. Cu appears to enhance the desorption of H_2 via the migration of H species from basic to Cu sites and makes the basic sites available for subsequent C-H bond activation steps. Addition of CO_2 decreases the rate of base-catalyzed chain growth reaction to acetone, but does not affect the rate of ethanol dehydrogenation reaction on Cu metal sites

High-pressure isobutanol synthesis from CO/H_2 has been studied on 1 wt % K-$Cu_{0.5}Mg_5CeO_x$ catalysts at 593 K and 4.5 MPa. The catalyst deactivates continuously during the run, and CO conversion decreases from 12.5 % to 7.5 % after 140 h on stream. Methanol and isobutanol productivities decrease with the addition of 0.047 MPa of CO_2 into CO/H_2 feed. Methanol productivity recovers upon the removal of CO_2 from the feed. CO_2, however, irreversibly inhibits isobutanol production. Addition of 1-propanol to CO/H_2 feed increases isobutanol productivity on 1 wt % K-$Cu_{0.5}Mg_5CeO_x$ catalysts by an order of magnitude, suggesting that 1-propanol is the precursor to isobutanol.

The reduction behavior of a series of MgO-based Cu catalysts was investigated using temperature-programmed reduction. The presence of CeO_x decreases CuO reduction temperature, and the promoting effect of CeO_x on CuO reduction increases with increasing Ce/Mg ratio. In contrast to CeO_x, K addition to Cu-containing samples inhibits CuO reduction. The presence of K_2O in CuO may inhibit to some extent H_2 activation and increase the bond strength of CuO and therefore retard CuO reduction.

The density and strength of available basic sites have been determined using a $^{13}CO_2/^{12}CO_2$ isotopic exchange method. The number of available basic sites measured at different flow rate is similar; the slope of the transient curve, however, changes with flow rates due to the readsorption of $^{13}CO_2$. Mathematical treatment reveals that the curve slope is a function of both exchange rate constant and gas residence time.

The manuscript *"Isobutanol and Methanol Synthesis on Copper Catalysts Supported on Modified Magnesium Oxide"* has been submitted to the Journal of Catalysis for publication. A manuscript titled *"Isotopic Switch Methods for the Characterization of Basic Sites in Modified MgO Catalysts"* is in the final draft and will be submitted for publication during the next reporting period.

1. CONTRACT OBJECTIVES AND TASKS

The contract objectives are:

1. To design a catalytic material for the synthesis of isobutanol with a productivity of 200 g isoalcohols/g-cat-h and a molar isobutanol-to-methanol ratio near unity

2. To develop structure-function rules for the design of catalysts for the selective conversion of synthesis gas to isoalcohols

The research program has been grouped into five specific tasks and a set of project management and reporting activities. The abbreviated designations for these tasks are:

- Project Work Plan ***(Task 1)***

- Catalyst Synthesis ***(Task 2)***

- Catalyst Evaluation in Laboratory Scale Reactors ***(Task 3)***

- Identification of Reaction Intermediates ***(Task 4)***

- Bench-Scale Catalyst Evaluation at Air Products and Chemicals ***(Task 5)***

2. SUMMARY OF ACTIVITIES

Activities during this period have focused on:

- Preparation of a series of K-Cu/MgO/CeO_2, CuCoMgCeO_x, CuZnAlO_x, and Cu$MgAlO_x$ catalysts

- Kinetic studies of ethanol and acetaldehyde coupling reactions on K-Cu/MgO/CeO_2

- Investigation of the reduction behavior of MgO-based Cu catalysts

- Studies of the effect of total flow rate on the determination of basic site density and strength at reaction temperatures using $^{13}CO_2/^{12}CO_2$ switch methods

- Evaluation of high-pressure isobutanol synthesis reactions on K-$CuMg_5CeO_x$ catalysts

3. STATUS, ACCOMPLISHMENTS, AND RESULTS

Task 1: Management Plan

No activities were carried out during this reporting period.

Task 2: Catalyst Synthesis

$CuZnAlO_x$ (MG4-2 O) and $Cu_{0.5}Mg_5CeO_x$ (MG3-13 O) prepared in previous reporting periods were impregnated with Cs and K, respectively. These materials were prepared to verify the reproducibility in catalyst preparation and to provide large amounts of samples for CO_2 and alcohol addition and isotopic tracer studies in CMRU. The precursor (MG3-15 P) of Cu/Mg/Al samples provided by Dr. Carlos Apesteguia (UNL, Argentina) was calcined at 723 K for 4 h to obtain the mixed oxide (MG3-15 O). K- and Cs-promoted $CuMgAlO_x$ catalysts were prepared by incipient wetness of the oxidized samples using K_2CO_3 (0.25 M) and CH_3COOCs (0.25 M) aqueous solutions (K_2CO_3: Fisher Scientific, A.C.S. certified; CH_3COOCs: Stream Chemicals, 99.9%). Catalyst properties are summarized in *Table 1*.

Table 1. Composition and surface areas of metal oxides.

Sample	**Nominal composition**	**Alkali** (wt.%) AAS	**S.A.** (m^2 / g)
MG 4 - 2 O/Cs	1.2 wt % Cs-$CuZnAlO_x$	1.25	74
MG 3 - 13 O/K	1.0 wt % K-$Cu_{0.5}Mg_5CeO_x$	1.03	150
MG 3 - 15 O	$Cu_{0.5}Mg_5Al_{10}O_x$	0.05	327
MG 3 - 15 O/K	1.0 wt % K-$Cu_{0.5}Mg_5Al_{10}O_x$	1.15	264
MG 3 - 15 O/Cs	3.4 wt % K-$Cu_{0.5}Mg_5Al_{10}O_x$	2.88	258

Based on the catalyst composition reported by Keim [1] and more recently by Dombeck [2] for higher alcohol synthesis from CO and H_2, new catalytic materials containing Pd were prepared by incorporating Pd into the modified MgO catalysts (K-$Cu_{0.5}Mg_5CeO_x$ and K(Cs)-Mg_5CeO_x) in order to increase total alcohols and isobutanol productivities and isobutanol/methanol ratio. These samples will be tested in CMRU in the next reporting period.

Task 3: Catalyst Evaluation in Laboratory Scale Reactors

3.1. Kinetic Studies of Alcohol Coupling Reactions

Dehydrogenation and condensation reactions of ethanol were investigated on Mg_5CeO_x (MG3-7 O), $Cu_{0.5}Mg_5CeO_x$ (MG3-11 Ow), 1.0 wt % K-$Cu_{0.5}Mg_5CeO_x$ (MG3-11 Ow/K), and 1.2 wt % K-$Cu_{7.5}Mg_5CeO_x$ (MG3-6 Ow/K) in order to address the role of each individual catalyst component in chain growth reactions. The experiment was carried out in a gradientless

recirculating reactor unit (RRU). The catalyst (19.0 mg) was first reduced in H_2 (10 % H_2/He) at 623 K for 0.5 h. The temperature was lowered to 573 K and ethanol was introduced along with a small amount of methane, used as an unreactive internal standard (reaction mixture: $C_2H_5OH/CH_4/He$ = 4.0/2.7/94.6 kPa; C_2H_5OH: Fisher Scientific, A.C.S. certified; CH_4: Matheson, ultra high purity). Products were sampled by syringe extraction from the recirculating stream at different contact times, and injected into a gas chromatograph equipped with flame ionization and thermal conductivity detectors. Mass spectrometry after chromatographic separation was used to confirm the identity of each reaction product.

Acetaldehyde was the initial product of reactions of pure ethanol on 1 wt % K-$Cu_{0.5}Mg_5CeO_x$ (*Figure 1*). Dehydrogenation reactions occur much faster than the chain growth reactions to acetone, n-butyraldehyde, and other oxygenates. Acetaldehyde reaches a maximum concentration at intermediate contact times during ethanol reactions and then decreases gradually, suggesting that acetaldehyde is involved in subsequent chain growth reactions or reaches the equilibrium and is converted back to ethanol. Acetone and n-butyraldehyde were the predominant condensation products. The non-zero initial slopes of acetone and n-butyraldehyde curves are not expected for products formed through consecutive reactions. Therefore, acetone and n-butyraldehyde are formed either by ethanol condensation or by acetaldehyde condensation with zero-order kinetics. Methyl-ethyl ketone (by acetaldehyde condensation with oxygen retention reversal [3, 4], 2-pentanone (by acetaldehyde-acetone condensation), and ethyl acetate (by ethanol-acetaldehyde) were detected among reaction products in much smaller concentrations.

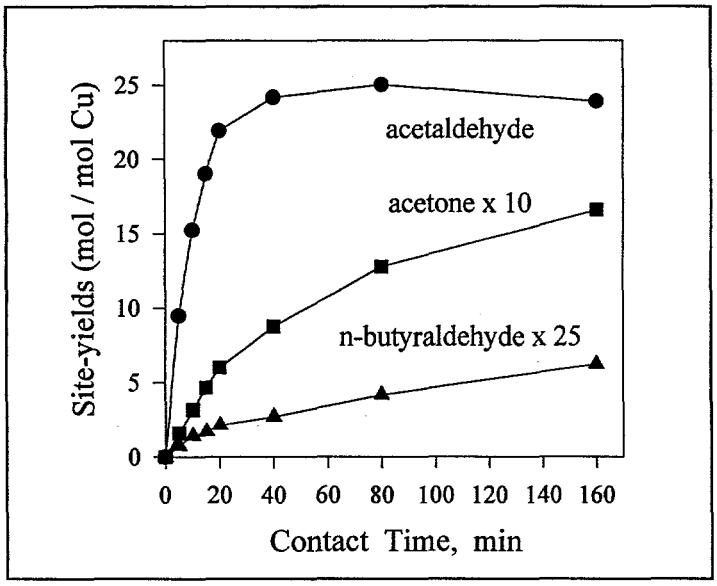

Figure 1. Site yields as a function of contact time on 1.0 wt % K-$Cu_{0.5}Mg_5CeO_x$ in ethanol reactions. [573 K, 101.3 kPa total pressure, 4.0 kPa ethanol, balance He].

Reaction pathways involved in the formation of all detected products are shown in *Figure 2*. Acetaldehyde is formed via ethanol dehydrogenation (step I) and undergoes subsequent condensation reactions (steps II-XII). The self-condensation of acetaldehyde by an aldol-type condensation produces n-butyraldehyde (steps II-IV) and methyl-ethyl ketone (steps

II-V) [3]. The aldol species is converted to the keto form via H transfer (step VI). The dehydration-dehydrogenation reactions of the keto form (step VII) lead to methyl-ethyl ketone. Acetone is formed via two pathways: by reaction of aldol intermediates with surface oxygen followed by decarboxylation (steps VIII-IX) and by reverse aldol condensation of the keto form (step X). Formaldehyde formed in the latter reaction decomposes rapidly to CO and H_2. 2-Pentanone is formed by condensation of aldol-type intermediates formed in acetone-acetaldehyde self condensation reactions (steps XI-XII). Ethylacetate forms via the reaction of ethanol and acetaldehyde (step XIII) [3].

The rates of ethanol conversion and acetaldehyde, n-butyraldehyde, and acetone formation were measured and the results are summarized in *Table 2*. Initial reaction rates were obtained from the slopes of site-yield plots at short contact times using total surface area, $MgCeO_x$ surface area (estimated from the difference between the total and the copper surface area), and Cu metal surface area of each sample.

Table 2. Effects of Cu- and K-loading on Ethanol Consumption and Product formation on Mg_5CeO_x.

wt. % Cu	wt. % K	Ethanol dehydrogenation areal rate $^{(1)}r_1$	Ethanol dehydrogenation Turnover rate $^{(2)}r_1$	Formation rates of Acetone $^{(3)}r_2$	Acetone $^{(4)}r_2$	Butyraldehyde $^{(3)}r_3$	Butyraldehyde $^{(4)}r_3$
0	0	1.3×10^{-8}	/	6.2×10^{-11}	6.5×10^{-5}	(5)	(5)
7	0.1	3.6×10^{-7}	0.24	3.0×10^{-9}	2.2×10^{-3}	4.5×10^{-10}	3.4×10^{-4}
7	1.0	2.4×10^{-7}	0.23	4.3×10^{-9}	1.8×10^{-3}	7.6×10^{-10}	3.2×10^{-4}
49	1.2	9.4×10^{-7}	0.24	4.4×10^{-8}	1.0×10^{-2}	1.2×10^{-9}	2.8×10^{-4}

(1) r_1 is the rate of ethanol consumption, and is expressed in mol/m^2 total · s.
(2) Turnover rates per Cu surface atom, and is expressed in s^{-1}.
(3) r_2 and r_3 are the rates of product formation, and are expressed in mol/m^2 $MgCeO_x$ · s.
(4) Turnover rates per accessible basic site from $^{13}CO_2/^{12}CO_2$ measurements and is expressed in mol/mol CO_2 exchangeable·s.
(5) Not detected.

Ethanol dehydrogenation rates were much higher on $Cu_{0.5}Mg_5CeO_x$, 1.0 wt % K-$Cu_{0.5}Mg_5CeO_x$, and 1.2 wt % K-$Cu_{7.5}Mg_5CeO_x$ catalysts than on Mg_5CeO_x, suggesting the involvement of Cu metal sites in the dehydrogenation of ethanol to acetaldehyde. The presence of K decreased areal ethanol dehydrogenation rates because of a concomitant decrease in Cu dispersion (4Q, FY1996). Ethanol dehydrogenation turnover rates (normalized by exposed Cu atoms) on $Cu_{0.5}Mg_5CeO_x$, 1.0 wt % K-$Cu_{0.5}Mg_5CeO_x$, and 1.2 wt % K-$Cu_{7.5}Mg_5CeO_x$ catalysts were 0.24, 0.23, and 0.24 s^{-1}, respectively. Thus, ethanol dehydrogenation occurs predominantly on exposed Cu atoms, which become inaccessible for both N_2O decomposition and alcohol dehydrogenation by blocking with K species. Dehydrogenation turnover rates were not affected by Cu crystallite size or by the titration of Cu surface atoms with K .

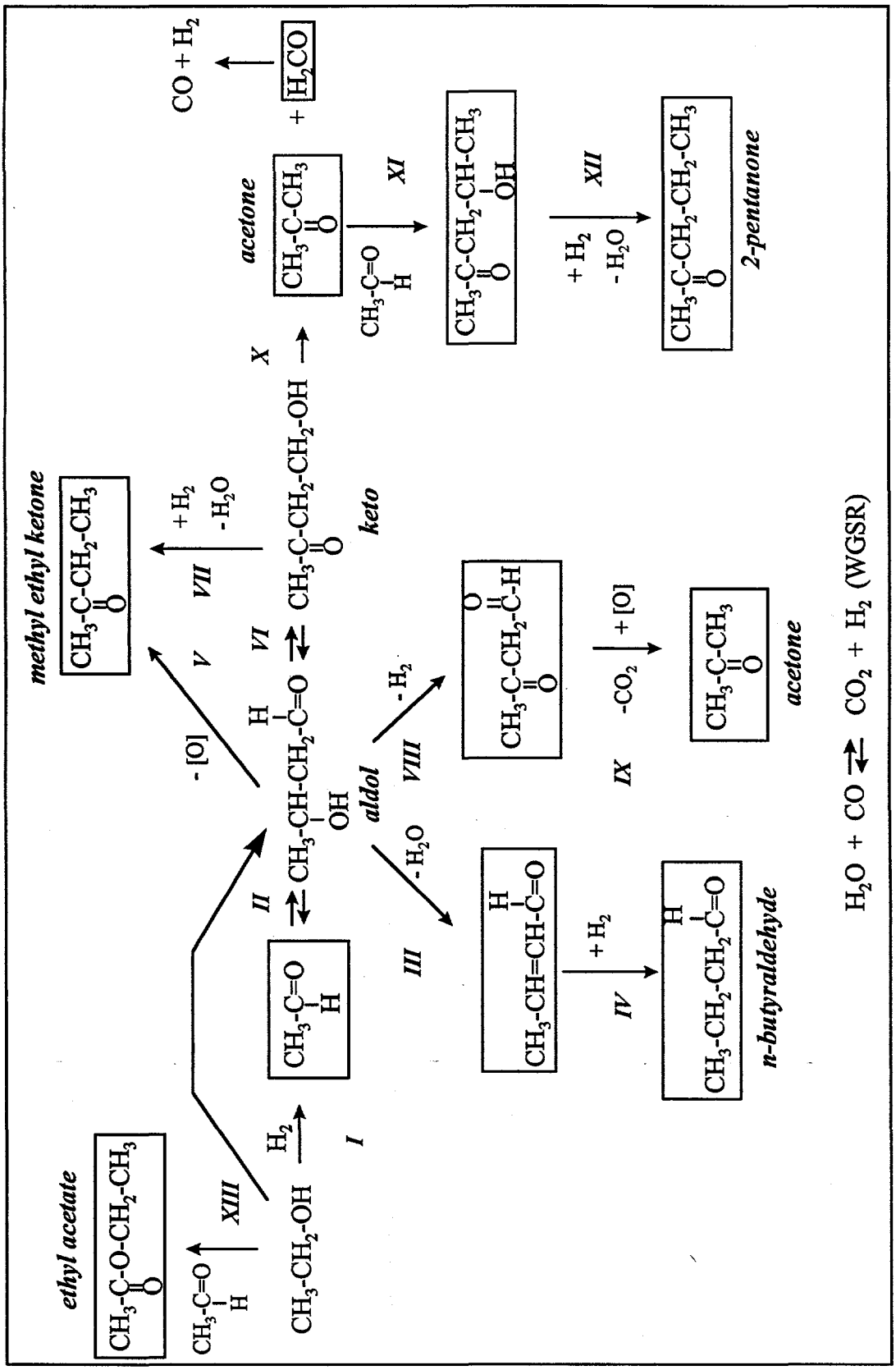

Figure 2. Reaction scheme for ethanol reactions.

Aldol coupling chain growth rates are lower on Mg_5CeO_x than on $Cu_{0.5}Mg_5CeO_x$ because of the lower acetaldehyde in the former. At similar steady-state acetaldehyde concentrations on $Cu_{0.5}Mg_5CeO_x$ and 1.0 wt % K-$Cu_{0.5}Mg_5CeO_x$ catalysts, the presence of K increases the rates of base-catalyzed aldol coupling reactions to acetone and butyraldehyde (*Table 2*). Thus, it appears that the higher basic site density and strength measured by $^{13}CO_2/^{12}CO_2$ isotopic switch measurements lead to higher rates of aldol condensation reactions. The rates of base-catalyzed aldol coupling reactions, when normalized by the number of accessible basic sites, are similar on $Cu_{0.5}Mg_5CeO_x$ (2.2×10^{-3} s^{-1}) and K-$Cu_{0.5}Mg_5CeO_x$ (1.8×10^{-3} s^{-1}). Aldol coupling chain growth reaction rates on 1.2 wt % K-$Cu_{7.5}Mg_5CeO_x$ (49 wt % Cu, 0.047 Cu dispersion) are, however, much higher than on K-$Cu_{0.5}Mg_5CeO_x$, even though basic site densities are similar on both samples. The difference in chain growth rates indicates that Cu metal sites are involved in rate-determining steps required for condensation reactions. This is confirmed by the lower aldol coupling reaction rates observed on Cu-free catalysts, which are caused not only by the lower concentrations of required acetaldehyde intermediates but also by the absence of Cu sites required in condensation steps.

The role of copper suggests a bifunctional mechanism for aldol condensation. Ethanol adsorbs dissociatively on MgO surface to form ethoxide and hydrogen species. Hydrogen species are removed by migration to Cu sites, reaction with another H species, and desorption as H_2:

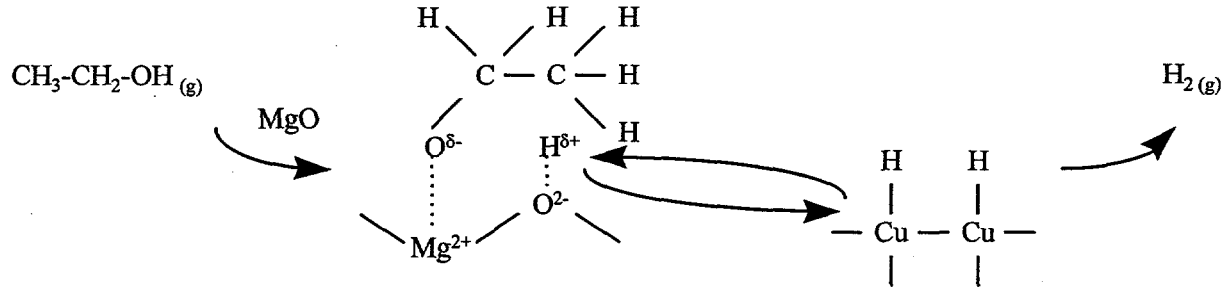

The ethoxide species then loses a β-H via intermolecular hydrogen transfer to oxygen ions and forms surface acetaldehydic species:

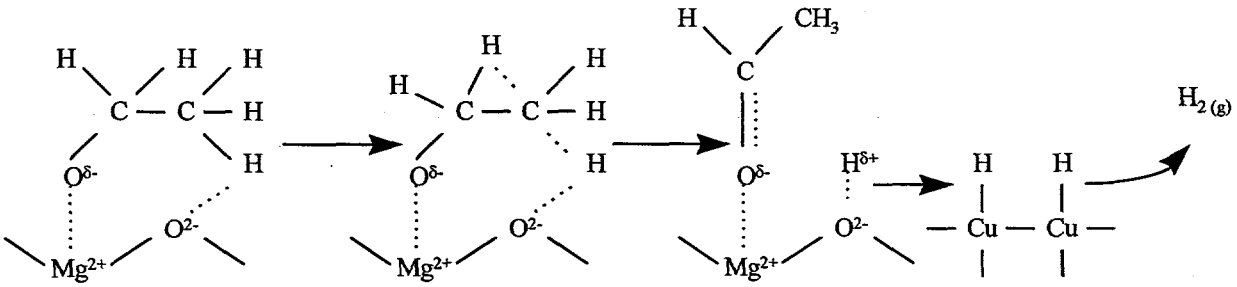

H species migrate from basic to Cu sites and recombine on Cu sites to form H_2; as a result, basic sites become available for another turnover. H-H recombination rates increase with increasing ratio of surface Cu atoms to basic sites, which is reflected in the ratio of Cu surface area to oxide surface area on K-$Cu_{7.5}Mg_5CeO_x$ (0.31) and K-$Cu_{0.5}Mg_5CeO_x$ (0.07) at similar basic site density. The high Cu-to-oxide surface area ratio on K-$Cu_{7.5}Mg_5CeO_x$ (0.31) leads to higher

aldol-condensation rates. Adsorbed acetaldehyde species can either desorb as acetaldehyde or react with other surface species to form aldol condensation products:

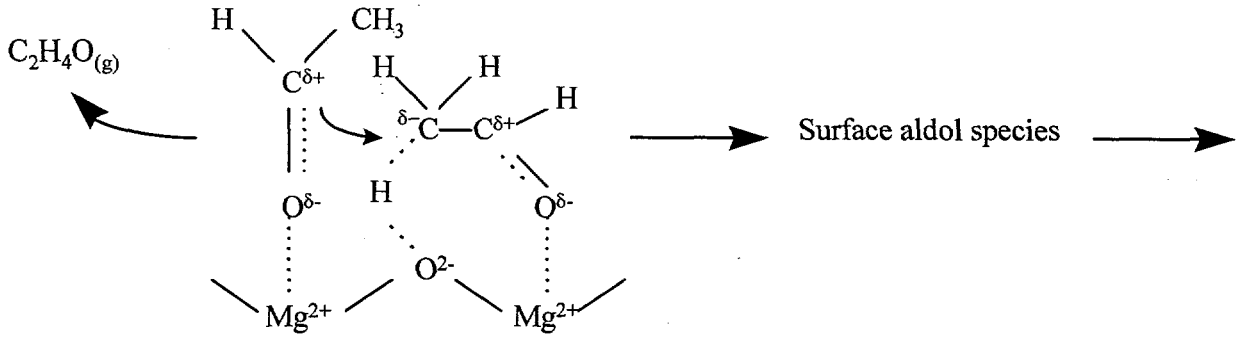

Surface aldol species can undergo further reactions via the pathways shown in *Figure 2*. In these reactions, the presence of copper sites enhances H mobility and provides H species for the hydrogenation of unsaturated species (steps IV, VII, and XII, *Figure 2*). It should be pointed out that the rates of the final products formed through consecutive reactions should have zero initial slopes, unless the formation of the product has a zero-order kinetics. The non-zero initial slopes of acetone and n-butyraldehyde curves (*Figure 1*) would be explained by the mechanism proposed above because it provides a pathway for direct conversion of ethanol to condensation products without the requirement for gas phase acetaldehyde.

The effect of CO_2 on ethanol dehydrogenation and coupling reactions was examined on a 1.0 wt % K-$Cu_{0.5}Mg_5CeO_x$ catalyst (19 mg) by adding CO_2 (3.5 kPa and 20.0 kPa) to ethanol/H_2 (4.0/29.3 kPa) reactant mixtures in a gradientless batch reactor. The results are shown in *Figure 3*. Ethanol dehydrogenation reaction rates do not change with increasing CO_2 pressure, suggesting that Cu sites were not inhibited by CO_2. Also, CO_2 does not affect the rate of n-butyraldehyde formation. These data are not consistent with the observed decrease in methanol and isobutanol synthesis rates as CO_2 is added to CO/H_2 feeds in CMRU. It appears that the higher CO_2 pressures under typical isobutanol synthesis conditions reduces the number of Cu sites required for alcohol synthesis. On catalyst compositions leading to selective methanol synthesis i.e., Cu/ZnO/Al_2O_3, the presence of CO_2 in modest concentrations (1-2 % mol) actually increases methanol synthesis rates [3]; higher CO_2 concentrations (>10% mol), however, lead to the oxidation of surface Cu atoms and consequently to the inhibition of methanol synthesis [3]. The strong inhibition effect of CO_2 on methanol synthesis rates has been reported for catalysts containing Cu and Ce [6]. Competitive adsorption between CO_2 and aldehyde on basic sites may account for the observed inhibition of condensation reactions on 1.0 wt % K-$Cu_{0.5}Mg_5CeO_x$ catalysts under high pressure isobutanol synthesis conditions. The ratio of CO_2 and aldehydic intermediates is much higher under the high-pressure isobutanol synthesis conditions than in low-pressure ethanol reaction experiments, because of the lower aldehyde/alcohol ratio at higher H_2 pressure in the former. CO_2 competition for basic sites, therefore, is not favorable and aldol coupling reactions are not influenced strongly by CO_2 in the former. The rate of acetone formation, however, decreased when CO_2 was present during ethanol reactions. CO_2 inhibition effect on acetone production could be a result of several factors: 1) the presence of CO_2 reverses the reaction step that forms acetone and CO_2 (steps IX

and X, Fig. 9), or 2) acetone is produced following a different parallel reaction path using stronger basic sites which are inhibited by CO_2.

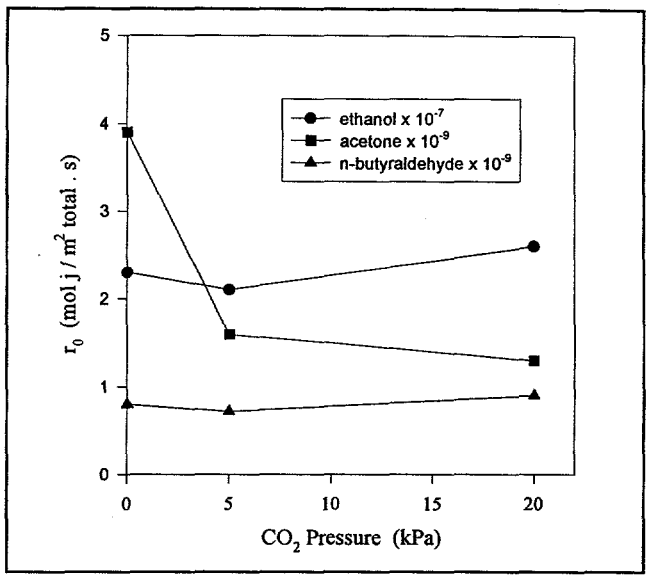

Figure 3. Rates of ethanol consumption and product formation as a function of CO_2 initial pressure on 1.0 wt % K-$Cu_{0.5}Mg_5CeO_x$. [573 K, 101.3 kPa total pressure, 4.0 kPa ethanol, 26.7 kPa dihydrogen, balance He].

Condensation and hydrogenation reactions of acetaldehyde were investigated on 1.0 wt % K-$Cu_{0.5}Mg_5CeO_x$ (MG3-11 Ow/K) and 1.2 wt % K-$Cu_{7.5}Mg_5CeO_x$ (MG3-6 Ow/K) in a gradientless recirculating reactor unit (RRU). These experiments were performed in order to determine whether Cu sites are required for acetaldehyde reactions, as proposed previously for ethanol reactions.

Catalytic activity and product yields for acetaldehyde reactions on 1.0 wt % K-$Cu_{0.5}Mg_5CeO_x$ and 1.2 wt % K-$Cu_{7.5}Mg_5CeO_x$ are shown in *Figure 4*. Acetone and crotonaldehyde are the predominant condensation products. Carbon dioxide, n-butyraldehyde, methyl propenyl ketone, and 2-pentanone were also detected in small concentrations among reaction products. Ethanol was the product of acetaldehyde hydrogenation. An aldol-type self-condensation of acetaldehyde produced crotonaldehyde, some of which is hydrogenated to n-butyraldehyde. Acetaldehyde may also polymerize to yield dimer and trimer compounds, which remained on the catalyst surface and led to poor mass balances (<50 %). Reaction pathways involved in the formation of the all observed products are shown in *Figure 5*.

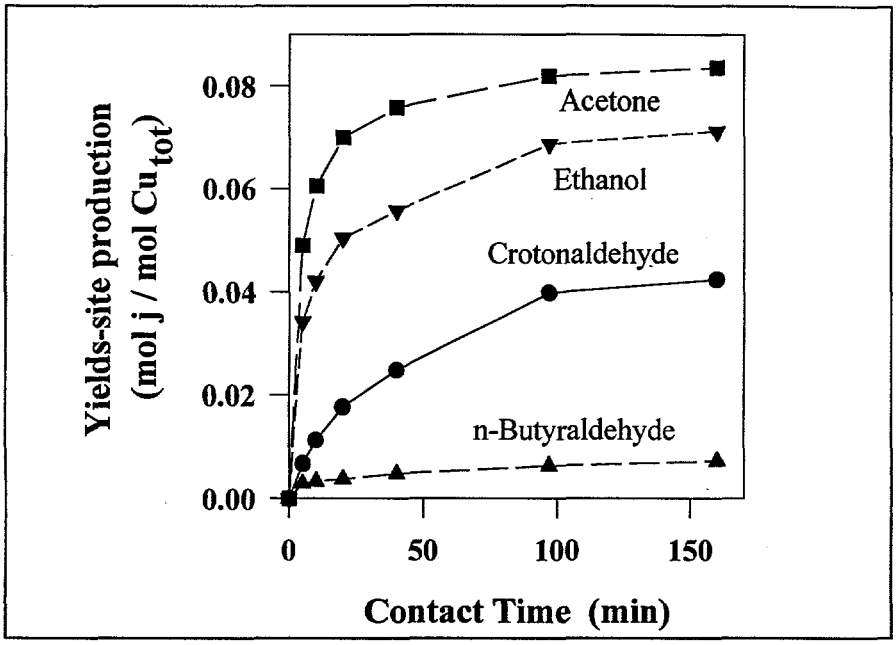

Figure 4. Acetaldehyde reactions. Site yields as a function of contact time on 1.2 wt. % K-$Cu_{7.5}Mg_5CeO_x$. [573 K, 101.3 kPa total pressure, 7.0 kPa acetaldehyde, balance He].

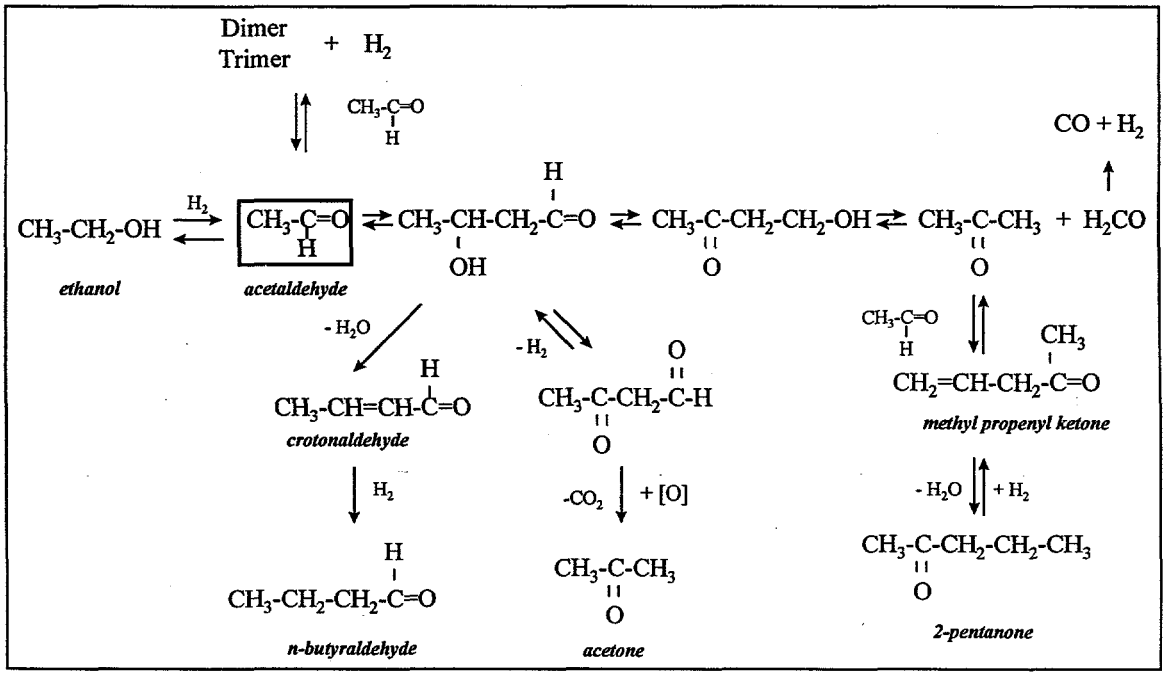

Figure 5. Reaction scheme for acetaldehyde reactions.

Hydrogenation products such as ethanol and n-butyraldehyde were formed by using H_2 generated in acetaldehyde polymerization reactions:

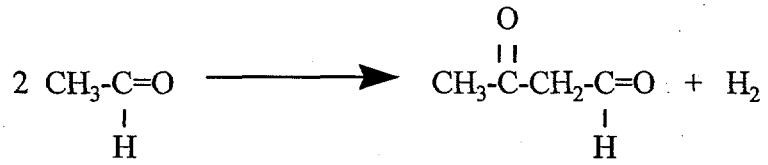

acetaldehyde **dimer**

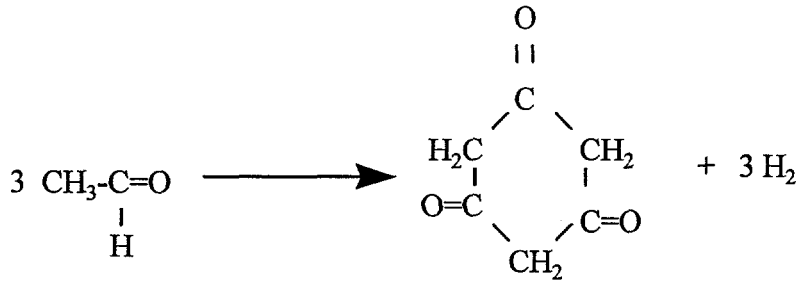

trimer

The initial reaction rates for acetaldehyde consumption and product formation on the low- and high-Cu catalysts are listed in *Table 3*. The rates of acetaldehyde consumption and acetone formation are higher on high Cu catalysts than on low Cu catalysts. Since the basicity of these two samples is comparable acetaldehyde reaction rate increases with increasing Cu loading possibly due to the enhancement of H mobility by Cu sites. The lower turnover rates of ethanol formation on high Cu catalysts may be caused by the limited supply of H atoms from acetaldehyde polymerization reactions.

Table 3. Effects of Cu on the rates of acetaldehyde consumption and product formation on 1.0 wt % K-$Cu_{0.5}Mg_5CeO_x$ and 1.2 wt % K-$Cu_{7.5}Mg_5CeO_x$.

wt % Cu	wt % K	Formation rates of [(1)]Aceladehyde	[(2)]Ethanol	[(3)]Crotonaldehyde	[(3)]Acetone
7	1.0	8.2×10^{-8}	4.8×10^{-3}	2.3×10^{-9}	4.0×10^{-9}
49	1.2	1.3×10^{-7}	2.4×10^{-3}	2.5×10^{-9}	1.8×10^{-8}

(1) Rate of acetaldehyde consumption, in mol/m^2 total · s.
(2) Turnover rates per Cu surface atom, in s^{-1}.
(3) Rates of product formation, in mol/m^2 base · s.

The effect of acetaldehyde partial pressure (3.1-14.6 kPa) on acetaldehyde reaction rates and product selectivity has been investigated on 1.0 wt % K-$Cu_{0.5}Mg_5CeO_x$ (MG3-11 Ow/K) in order to determine the reaction order with respect to acetaldehyde partial pressure. The reaction was carried out at 573 K with a reaction mixture of $C_2H_4O/CH_4/He$ = 7.0/2.7/90.6 kPa (C_2H_4O:

Fisher Scientific, Reagent Grade; CH_4: Matheson, ultra high purity). Methane was used as an unreactive internal standard.

The initial reaction rates at different initial partial pressures of acetaldehyde are shown in *Figure 6*. The reaction rates of condensation products (acetone and crotonaldehyde) depend on the initial partial pressure of acetaldehyde. Kinetic reaction orders of 0.7 for crotonaldehyde and 0.8 for acetone were obtained by employing a like power law kinetic expression ($r_j=k_j.P_{acetal}^{n}$). These results indicate that the reaction kinetics is not zero-order with respect to acetaldehyde, as suggested previously for ethanol reactions on a similar catalyst.

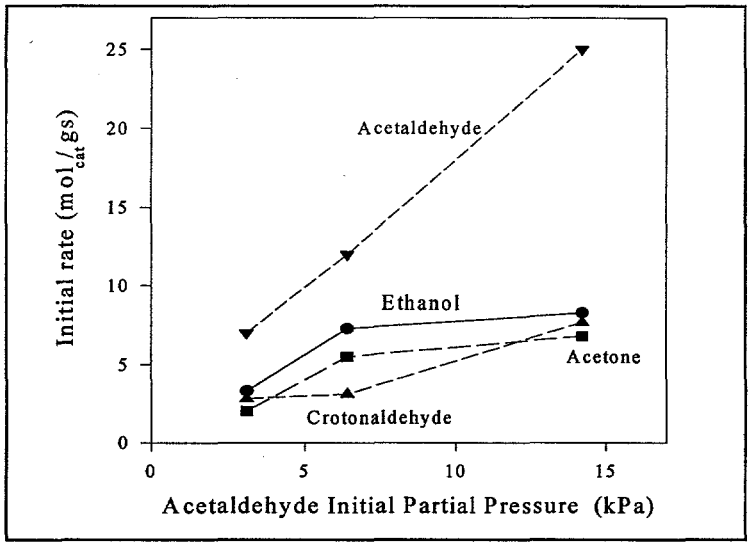

Figure 6. Effect of acetaldehyde partial pressure on the initial rates of acetaldehyde reaction and product formation 1.0 wt % K-$Cu_{0.5}Mg_5CeO_x$. [573 K, 101.3 kPa total pressure, 3-15 kPa acetaldehyde, balance He].

Competitive reactions between $^{12}C_2H_5OH$ and $^{13}C_2H_4O$ were examined on a 1.0 wt % K-$Cu_{0.5}Mg_5CeO_x$ (MG3-11 Ow/K) in order to probe the mechanistic significance of the non-zero initial rate of acetone formation in ethanol dehydrogenation and coupling reactions. The catalyst (20 mg) was charged into a gradientless batch reactor. The sample was reduced in 10 % H_2 (balance He) at 623 K for 0.5 h. Reactions were conducted at 523 K and 101.3 kPa in a recirculating reactor unit (RRU) with a reaction mixture of $^{13}C_2H_4O/^{12}C_2H_5OH/H_2/CH_4/He$ = 1.3/3.7/21.2/2.4/72.7 kPa. ($^{13}C_2H_4O$: Isotec Inc., 2 ^{13}C: 99 %; C_2H_5OH: Fisher Scientific, A.C.S. certified; CH_4: Matheson, ultra high purity). The results are shown in *Figures 7* and *8*.

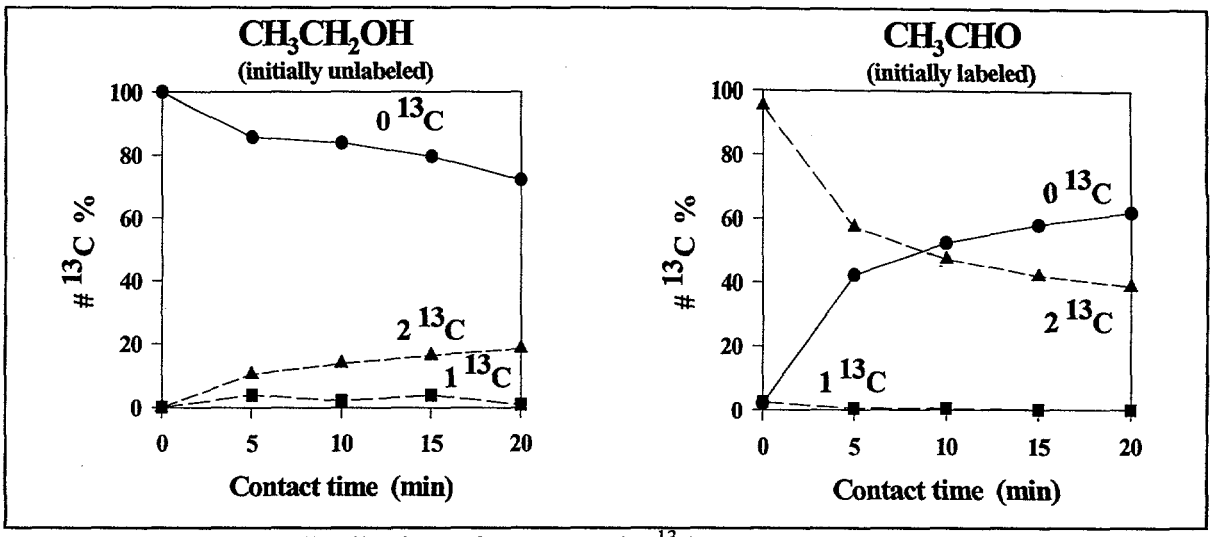

Figure 7. Carbon-13 distribution of reactants in $^{13}C_2H_4O$-C_2H_5OH-H_2 reactions on 1.0 wt % $Cu_{0.5}Mg_5CeO_x$ as a function of contact time. [523 K, 101.3 kPa total pressure, 1.3 kPa acetaldehyde, 3.7 kPa ethanol, balance He].

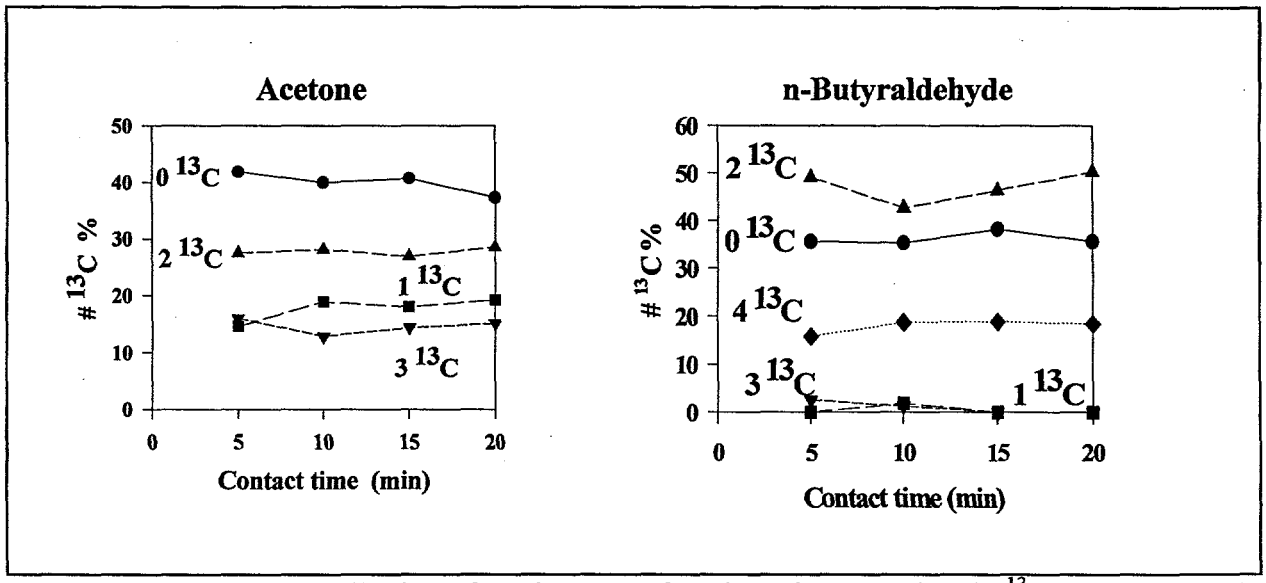

Figure 8. Carbon-13 distribution of products as a function of contact time in $^{13}C_2H_4O$-C_2H_5OH-H_2 reactions on 1.0 wt % K-$Cu_{0.5}Mg_5CeO_x$. [523 K, 101.3 kPa total pressure, 1.3 kPa acetaldehyde, 3.7 kPa ethanol, balance He].

The carbon-13 distributions of products showed in *Figure 8* do not change with contact time, but the carbon-13 distributions in reactants change significantly (*Figure 7*), suggesting that the reactants may form polymer species on the surface, which decompose to give the observed products. From the total carbon-13 content we are not able to determine if acetone (40% of ^{13}C, 1.2 ^{13}C) or n-butyraldehyde (40% of ^{13}C, 1.7 ^{13}C) comes from ethanol or acetaldehyde (reaction mixture contents 26.5% of ^{13}C) because both lose their isotopic identities.

Dehydrogenation and condensation reactions of ethanol were investigated on a physical mixture of K-Mg_5CeO_x (MG3-7 O/K) and 1.2 wt % K-$Cu_{7.5}Mg_5CeO_x$ in order to address whether the proximity between Cu and basic sites are required for the base-catalyzed condensation reactions. This physical mixture was prepared in order to simulate the low-Cu catalyst (same number of Cu sites and the same number of basic sites as it had in 1.0 wt % K-$Cu_{0.5}Mg_5CeO_x$ sample). The catalyst (22.8 mg) was first reduced in H_2 (10% H_2/He) at 623 K for 0.5 h. The temperature was lowered to 573 K and ethanol was introduced along with a small amount of methane, used as an unreactive internal standard (reaction mixture: C_2H_5OH/CH_4/He = 4.0/2.7/94.6 kPa; Fisher Scientific: C_2H_5OH A.C.S. certified; Matheson: CH_4 ultra high purity).

Acetaldehyde was the initial reaction product of pure ethanol feeds on $Cu_{0.5}Mg_5CeO_x$ (*Figure 9*). Dehydrogenation reactions occur much faster than the chain growth reactions to acetone, n-butyraldehyde, and other oxygenates on all the catalysts tested. The initial reaction rates for acetaldehyde reaction and product formation are shown in *Table 4*. The turnover rate of ethanol dehydrogenation on the physical mixtures was surprisingly twice as much as that observed on low and high-Cu catalysts. No explanation was found for this result. The rate of acetone formation on high-Cu catalysts was higher than that on low-Cu catalyst and the physical mixture, suggesting that the proximity between Cu and basic sites favors the production of acetone, but not n-butyraldehyde. On the other hand, n-butyraldehyde formation rate is an order of magnitude higher for the physical mixture than for the low or high Cu catalysts.

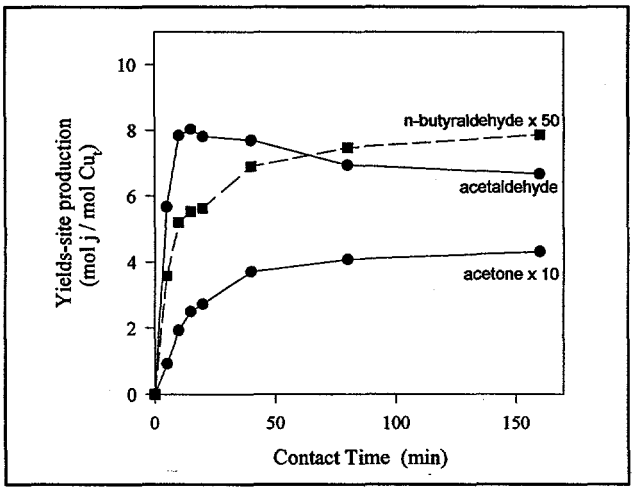

Figure 9. Ethanol reactions. Site yields as a function of contact time on a physical mixture of K-Mg_5CeO_x (MG3-7 O/K) and 1.2 wt % K-$Cu_{7.5}Mg_5CeO_x$. [573 K, 101.3 kPa total pressure, 3.5 kPa ethanol, balance He].

Table 4. Effect of the proximity between Cu and basic sites on ethanol consumption and product formation on 1.0 wt % K-$Cu_{0.5}Mg_5CeO_x$, 1.2 wt % K-$Cu_{7.5}Mg_5CeO_x$, and a physical mixture of K-Mg_5CeO_x and 1.2 wt % K-$Cu_{7.5}Mg_5CeO_x$.

Catalyst	Ethanol dehydrogenation		Formation rates of			
	areal rate	Turnover rate	Acetone		Butyraldehyde	
	$^{(1)}r_1$	$^{(2)}r_1$	$^{(3)}r_2$	$^{(4)}r_2$	$^{(3)}r_3$	$^{(4)}r_3$
low-Cu	2.4×10^{-7}	0.23	4.3×10^{-9}	1.8×10^{-3}	7.6×10^{-10}	3.2×10^{-4}
high-Cu	9.4×10^{-7}	0.24	4.4×10^{-8}	1.0×10^{-2}	1.2×10^{-9}	2.8×10^{-4}
mixture	4.6×10^{-7}	0.46	6.9×10^{-9}	3.1×10^{-3}	5.2×10^{-9}	2.4×10^{-3}

(1) r_1 is the rate of ethanol consumption, and is expressed in mol/m^2 total · s.
(2) Turnover rates per Cu surface atom, and is expressed in s^{-1}.
(3) r_2 and r_3 are the rates of product formation, and are expressed in mol/m^2 $MgCeO_x$ · s.
(4) Turnover rates per accessible site from $^{13}CO_2/^{12}CO_2$ and is expressed in mol/mol CO_2 exchangeable·s.

3.2. Isobutanol Synthesis at High Pressure in CMRU

3.2.1. Methanol turnover rates

Table 5 shows methanol turnover rates found for some methanol synthesis catalysts in the literature [7-10] and for the most recent CMRU runs. The methanol turnover rates for the CMRU runs are calculated at a gas hourly space velocity of 6000 $cm^3/g/h$. All literature values are measured at lower temperature (493-523 K) and at different feed gas compositions compared to our catalysts. Both the low- and high-Cu K-$CuMgCeO_x$ catalysts, and the catalyst without Ce give similar methanol turnover rates. This is consistent with the fact that methanol productivity is proportional to Cu surface sites.

Table 5. Methanol synthesis turnover rates .

	Catalyst	Methanol turnover rate [mmol MeOH/mol Cu s]	Ref.
Litterature[1]	Cu/ZnO	15.7	[7]
	Cu/Zn/Al	15.7	[8]
	Cu/SiO_2	4.2	[9]
This study[2]	$Cu_{0.5}Mg_5O_x$[#]	9.0	run 22
	K-$Cu_{0.5}Mg_5CeO_x$[*]	7.9	run 19
	K-$Cu_{0.5}Mg_5CeO_x$[*]	8.2	run 20
	K-$Cu_{0.5}Mg_5CeO_x$[**]	9.1	run 23
	K-$Cu_{0.5}Mg_5CeO_x$[**]	8.9	run 24
	K-$Cu_{7.5}Mg_5CeO_x$	8.7	run 21

[1] 493-523 K, 5-7 MPa, $CO_2/CO/H_2$ feeds. [2] 593 K, 4.5 MPa, 6000 cm^3/g_{cat} h. [*] MG3-11 Ow/K
[**] MG3-13 O/K. [#] Incorrect value and catalyst identity reported in the November monthly report

3.2.2. *Deactivation during CMRU-23*

The plot of CO conversion versus time on stream (*Figure 10*) reveals that the catalyst deactivates continuously during the run. The deactivation rate decreases with time but the catalyst is still loosing activity after 14 days on-stream. The solid symbols represent the data obtained at 593 K and the open symbols at 603 K. It can be seen that an increase in the temperature by 10 K has essentially no effect on CO conversion when the deactivation is taken into account. Methanol selectivity, however, decreases with increasing temperature, resulting in a decrease in methanol yield. This is similar to what was found by Apesteguia et. al. [11]. They found essentially no change in CO conversion but a decrease in methanol selectivity with increasing temperature. The decrease in methanol yield is probably caused by lower equilibrium conversion levels for methanol synthesis at higher temperature.

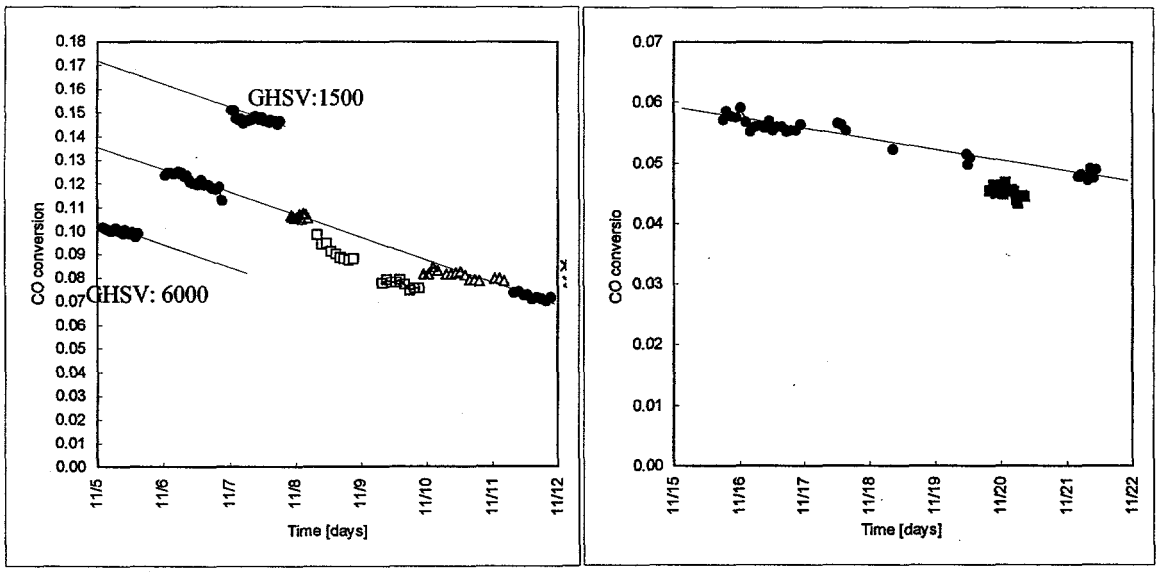

Open symbols: 603 K
Filled symbols: 593 K
Squares: CO2-addition

Figure 10. CO conversion vs. time-on-stream on 1 wt% K-$Cu_{0.5}Mg_5CeO_x$ catalysts (MG3-13 O/K). (593-603 K, 4.5 MPa, $H_2/CO = 1$, GHSV = 1500-6000 $cm^3/g/h$).

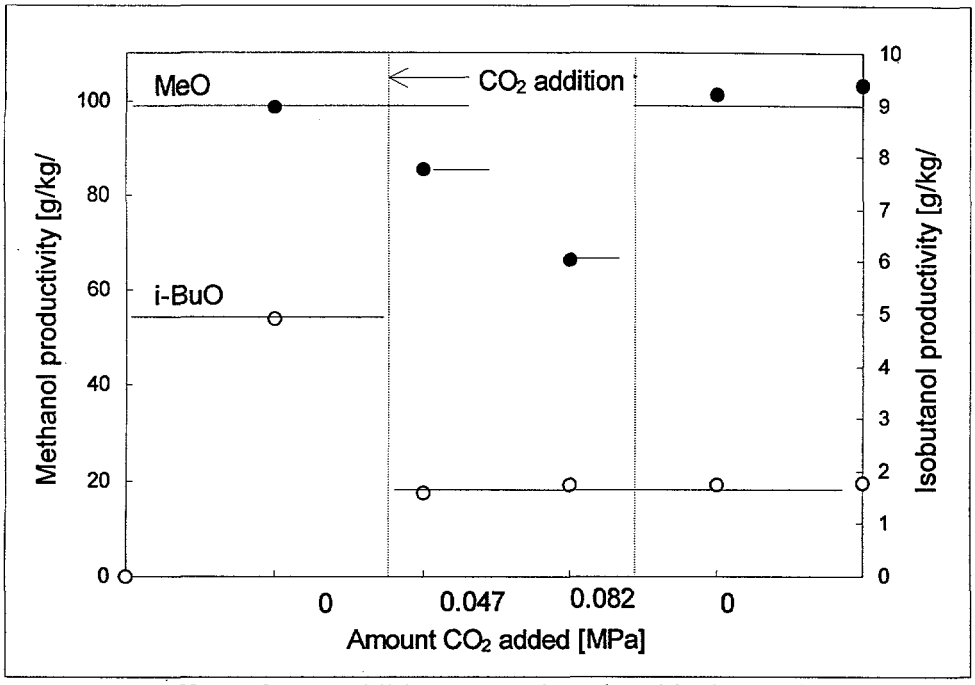

Figure 11. Effect of CO_2 addition on methanol and isobutanol productivities (after corrected for deactivation). ($H_2/CO = 1$, T = 603 K, P = 4.5 MPa, GHSV = 3000 cm^3/g cat/h).

Figure 11 shows the changes in methanol and isobutanol productivities when CO_2 is added to the feed gas. The CO conversion used for calculating the productivities has been corrected for the observed deactivation with time. When 0.047 MPa of CO_2 is added to the feed, isobutanol productivity is reduced to about 1/3 of the value before CO_2 addition. No further decrease was observed when the amount of CO_2 added was increased to 0.082 MPa, and the productivity was not recovered when the CO_2 addition was stopped. This suggests that the basic sites are irreversibly poisoned. The procedures for CO_2 addition were different for this run compared to earlier CO_2 addition runs for which no irreversible poisoning was detected. In this case the CO_2 was added directly during synthesis (without flushing the catalyst with H_2 before and after the CO_2 addition). The space velocity was kept constant and CO_2 added at two different levels in contrast to earlier runs where CO_2 was added in a certain amount and the space velocity was varied during the CO_2 addition.

The methanol productivity also decreased when CO_2 was added, but the productivity was recovered when the CO_2 addition was stopped. CO_2 seems to reversibly inhibit the methanol productivity. It is possible that the added CO_2 results in the oxidation of Cu (either directly or via H_2O). When the CO_2 is removed, the same $CO/H_2/CO_2/H_2O$ ratio as before is recovered, the Cu is reduced back again. It is also possible that the water-gas-shift reaction could influence on the measured CO conversion by converting some of the added CO_2 to CO. A decreased CO_2 selectivity would then be expected. Instead, an increased CO_2 selectivity was observed in the current run (possibly due to the uncertainty in correcting the measured CO_2 for the CO_2 added).

After the CO_2-addition studies, the catalyst had lost over 50% of its original activity and the CO conversion was so low that accurate measurements were difficult. It was therefore

decided to end the experiment at this point. After the experiment was ended the catalyst was removed from the reactor in four sections from the inlet of the reactor to the outlet. This was done in order to detect whether the extent of catalyst deactivation depends on its position in the reactor.

The total BET surface areas of the various portions of the used catalyst were measured. The results are presented in Table 6. The total surface area decreased to almost the half of the surface area of the fresh catalyst. If the catalyst deactivated only due to oxidation of Cu during reaction, a large decrease in total surface area is unlikely and sintering of the support seems therefore to be a more likely explanation. The reduction in total surface area could, however, be caused both by pore blocking by coke and by sintering of the catalyst, and it is not possible to discriminate between these two causes by the BET measurements. No difference could be detected between the inlet and outlet section of the catalyst bed by the BET measurements.

Table 6. BET surface area measured before and after methanol-isobutanol synthesis (CMRU 23).

MG3-13 O/K	BET surface area [m^2/g cat.]	Cu dispersion (%)
Fresh catalyst	150	15.8
Used catalyst - Inlet	84	3.6
Used catalyst - Outlet	85	1.2
[a]Used catalyst - Inlet	84	20.6

[a] After O_2 treatment at 723 K

A new sample of catalyst MG3-13 O/K was charged to the CMRU in order to carry out ethanol and propanol addition studies. This also provides an additional test of the reproducibility of the CMRU unit since a sample of the same batch of 1.0 wt % K-$Cu_{0.5}Mg_5CeO_x$ catalyst was charged. The same amount of catalyst as in CMRU-23 was charged and initially the same space velocity study was performed. *Figure* 12 shows the conversion and selectivities for the two comparable runs (CMRU-23 and -24) and Table 7 shows comparison of the two runs at 6000 cm^3/g-cat·h. The reproducibility is excellent, but a somewhat lower isobutanol (3.2 % vs. 4.3 % at 10 % conversion) and higher hydrocarbon selectivity (5.9 vs. 4.7 %) were observed in CMRU-24.

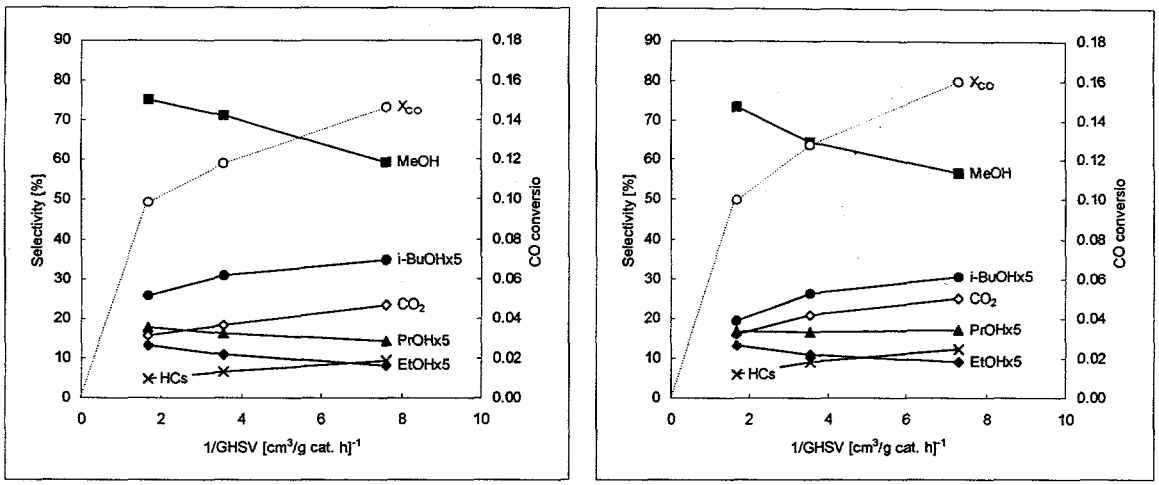

Figure 12. CO conversion and product selectivities for CMRU-23 and -24. [Catalyst: 1%K-$Cu_{0.5}Mg_5CeO_x$, 2.06 g, 4.5 MPa, 593 K, $H_2/CO=1$, 1500-6000 $cm^3/g\text{-}cat\cdot h$.]

Table 7. Comparison of CMRU-23 and -24. [Catalyst: 1wt % K-$Cu_{0.5}Mg_5CeO_x$, 2.06 g, 4.5 MPa, 593 K, $H_2/CO=1$, 6000 $cm^3/g\text{-}cat\cdot h$.]

RUN	CMRU-23	CMRU-24
Catalyst	MG3-13O/K	MG3-13O/K
amount [g]	2.06	2.06
GHSV [cm^3/g cat. h]$^{-1}$	6000	6000
CO conversion [%]	9.9	10.0
Rate of Reaction (mmol CO converted/g. cat.*hr.)	10.9	11.1
Methanol Productivity (g/kg*hr)	227.8	224.2
Isobutanol Productivity (g/kg*hr)	7.5	5.6
Selectivities (CO_2-free)		
CO_2 (%C)	15.6	16.1
Methanol	75.2	73.5
Ethanol	2.6	2.6
1-Propanol	3.6	3.4
Isopropanol	1.0	1.3
2-butanol	0.07	0.15
Isobutanol	4.3	3.2
1-butanol	0.00	0.27
1-pentanol	0.18	0.11
2-methyl-1-butanol	0.49	0.48
2-methyl-2-butanol	0.12	0.18
2-methyl-1-pentanol	0.14	0.14
1-hexanol	0.00	0.00
2-methyl-1-hexanol	0.02	0.00
Methane	3.6	4.4
C_{2+} Paraffins	1.1	1.5
Alcohols Selectivity	88.9	86.6
Paraffins Selectivity	4.7	5.9

After decreasing the space velocity from 6000 to 1500 cm^3/g-cat·h, the space velocity was increased again to 6000 cm^3/g-cat·h and then decreased to 3000 cm^3/g-cat·h. The results showed that the catalyst had deactivated. The CO conversion decreased from 10% to 7.5% at 6000 cm^3/g-cat·h (*Figure 13*). Both the methanol and isobutanol yield decreased.

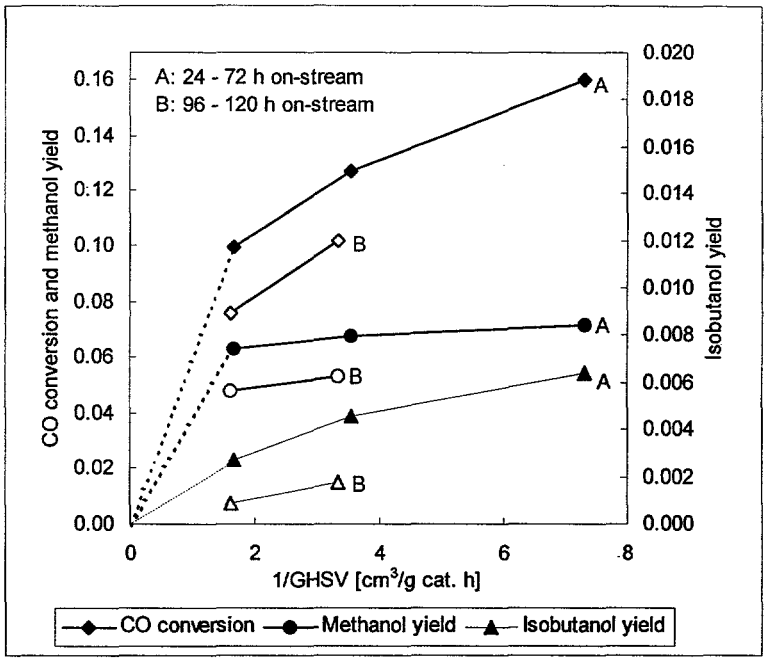

Figure 13. CO conversion, methanol and isobutanol yields as a function of space velocity and time. [CMRU-24, 593 K, 45 MPa, H_2/CO=1, 1500-6000 cm^3/g-cat·h.]

3.3.3. 1-Propanol addition

1-Propanol addition were studied earlier on high Cu catalysts. In this case, 1-propanol was added to the syngas feed for the low Cu-containing catalyst (1 wt % K-$Cu_{0.5}Mg_5CeO_x$) after initial space velocity studies. The amount of 1-propanol added was much higher than the amount of methanol produced due to experimental problems. It was originally intended to add about 20% of the methanol produced. The large amounts of alcohol added possibly result in a more pronounced competition with CO for active sites, resulting in a decrease in CO conversion. Only a slight decrease was observed previously when less propanol was added for the high Cu-containing catalyst.

The propanol was degassed with inert gas before it was charged to the pump and the alcohol was added to the feed after first measuring catalyst activity without propanol addition. Catalyst activity was also measured after propanol addition. The results are shown in Table 8. Isobutanol selectivity increased by an order of magnitude when propanol was added to the feed. The significant increase in isobutanol selectivity upon propanol addition is consistent with earlier results from this group and also with results reported for other higher alcohol catalysts (Cs-Cu/ZnO/Cr_2O_3) by Campos-Martin et al. [12]. Isobutanol is formed by condensation of C_1 intermediate derived from methanol or CO and 1-propanol or propionaldehyde. A large

increase in propane selectivity was observed as a result of the high amount of propanol added. Propene forms by dehydration of propanol.

The selectivity to 2-methyl-1-alcohols also increased with propanol addition. 2-methyl-1-butanol forms by the condensation of C_1 with 1-butanol and 2-methyl-1-pentanol forms by the self-condensation of 1-propanol. The experiment has to be repeated with the addition of smaller amounts of 1-propanol.

Table 8. Product selectivities and productivities on MG3-13 O/K (1 wt % K-$Cu_{0.5}Mg_5CeO_x$) with and without 1-propanol addition (593 K, 4.5MPa, H_2/CO=1, 3000 cm^3/g-cat·h).

	Without PrOH	with PrOH	Without PrOH
CO Conversion (%)	6.75	5.26	6.30
Rate of Reaction (mmol CO converted/g. cat.*hr.)	3.73	2.90	3.48
Methanol Productivity (g/kg*hr)	70.8	57.3	63.2
Isobutanol Productivity (g/kg*hr)	0.65	7.6	0.98
Selectivities (C%)			
CO_2	21.5	32.7	24.9
Propane(+propene)	4.9	24.4	5.7
methanol	59.3	61.7	56.1
ethanol	2.1	2.4	2.2
isopropanol	4.6	9.3	2.3
unknown	1.8	16.1	1.0
propanol	1.4	-	1.5
2-butanol	0.15	0.85	0.29
isobutanol	0.95	14.0	1.5
1-butanol	0.05	1.24	0.03
2-methyl-1-butanol	0.00	0.77	0.23
1-pentanol	0.08	0.86	0.23
2-methyl-1-pentanol	0.00	4.4	0.00
DME	7.2	2.5	6.8

In the next run Cs-CuZnAl (MG4-2O/Cs) will be tested. This type of catalyst has not been tested at the same conditions as most of K-CuMgCeO catalysts and an "in-house" prepared catalyst of this type has not been tested at all in the CMRU. After this, K-CuMgAl (Mg3-15O/K) and Cs-CuMgAl (Mg3-15O/Cs) will be tested followed by Co- and Pd-promoted modified MgO.

Task 4: Identification of Reaction Intermediates

During this reporting period, a high-pressure catalytic microreactor has been built and attached to the temperature-programmed surface reaction unit for the study of higher alcohol synthesis from CO/H_2. This experiment will focus on the reaction mechanisms for higher alcohol formation especially the chain-growth pathways from C_1 to C_2 alcohols. To fulfill this objective, a mixture of $^{13}CO/H_2$ and CH_3OH will be used as reactants. ^{13}CO contained in a lecture bottle (2.0 MPa) was pressurized using H_2 to make a 1/1 $^{13}CO/H_2$ mixture. This mixture

with a total pressure of 4.0 MPa enables us to run the experiment with a catalyst charge of 1.5 g at 2.0 MPa and a GHSV of 750 cm^3/g-cat-h for 15 h. CH_3OH will be introduced by passing $^{13}CO/H_2$ mixtures through a saturator containing CH_3OH at a desired temperature. All the gas feeding lines after the saturator will be wrapped up with heating tapes to ensure no readsorption and condensation of reactants and products. A part of effluent will be analyzed in-situ by mass spectrometry and the remainder will be trapped and analyzed using GC-MS and liquid-phase NMR.

4.1. Temperature-Program Reduction of MgO-based Cu Catalysts

Temperature-programmed reduction (TPR) was carried out on MgO-based Cu catalysts in order to address the effects of K and CeO_x on the reducibility of CuO. The experiment was carried out by first pretreating the samples at 723 K in flowing He (100 cm^3/min) for 0.5 h to remove carbonates, water, and weakly bonded hydroxyl species. Reactor temperature was then lowered to below 313 K and 5 % H_2/He was introduced at a total flow rate of 100 cm^3/min (STP). The temperature was then increased linearly at a rate of 0.17 K/s and the formation of H_2O and the consumption of H_2 were monitored continuously by mass spectroscopy.

The reduction profiles of MgO-based Cu samples are shown in Figure 14. The onset and peak maximum temperatures for H_2 consumption and H_2O formation obtained on each sample appeared at the same temperature. The high-temperature tail of the H_2O peak is caused by a strong interaction between H_2O and MgO. This tail was not observed for the H_2 peak, but the signal-to-noise ratio of H_2 peak was lower than that of H_2O because of the high H_2 background pressure in the mass spectrometer.

The presence of CeO_x in $Cu_{0.5}Mg_5CeO_x$ decreases the reduction temperature of CuO (508 K to 436 K). CeO_x addition also increases Cu dispersion and decreases Cu particle size, apparently because of the strong interaction between Cu and CeO_x. The large Cu particles in $Cu_{7.5}Mg_5CeO_x$, however, can also be reduced at temperatures lower than on $Cu_{0.1}MgO_x$. The reduction profiles (Figure 14) suggest that the promoting effect of CeO_x on copper oxide reduction is stronger at higher Ce/Mg ratios. CeO_x as a promoter for metal oxide reduction has been reported previously for $Pd/CeO_2/Al_2O_3$ catalysts (13). The presence of CeO_x shifts the reduction temperature of PdO from 437 K to 376 K. Moreover, the reduction behavior of a $Pd/CeO_2/Al_2O_3$ sample prepared by the coprecipitation of Pd and cerium nitrates differs from that of a $Pd/CeO_2/Al_2O_3$ prepared by conventional successive impregnation of CeO_2 and Pd. Some reduction occurs at room temperature on the sample prepared by the coprecipitation methods as a consequence of a higher degree of PdO-CeO_x contact area (14). Lamonier *et al.* (15) have found that Cu^{2+} insertion into CeO_x occurs during the synthesis of $CuCeO_x$ samples by coprecipitation methods. Four different species, present as CuO monomers, dimers, clusters, and small particles have been detected in CuO/CeO_2 mixtures (15).

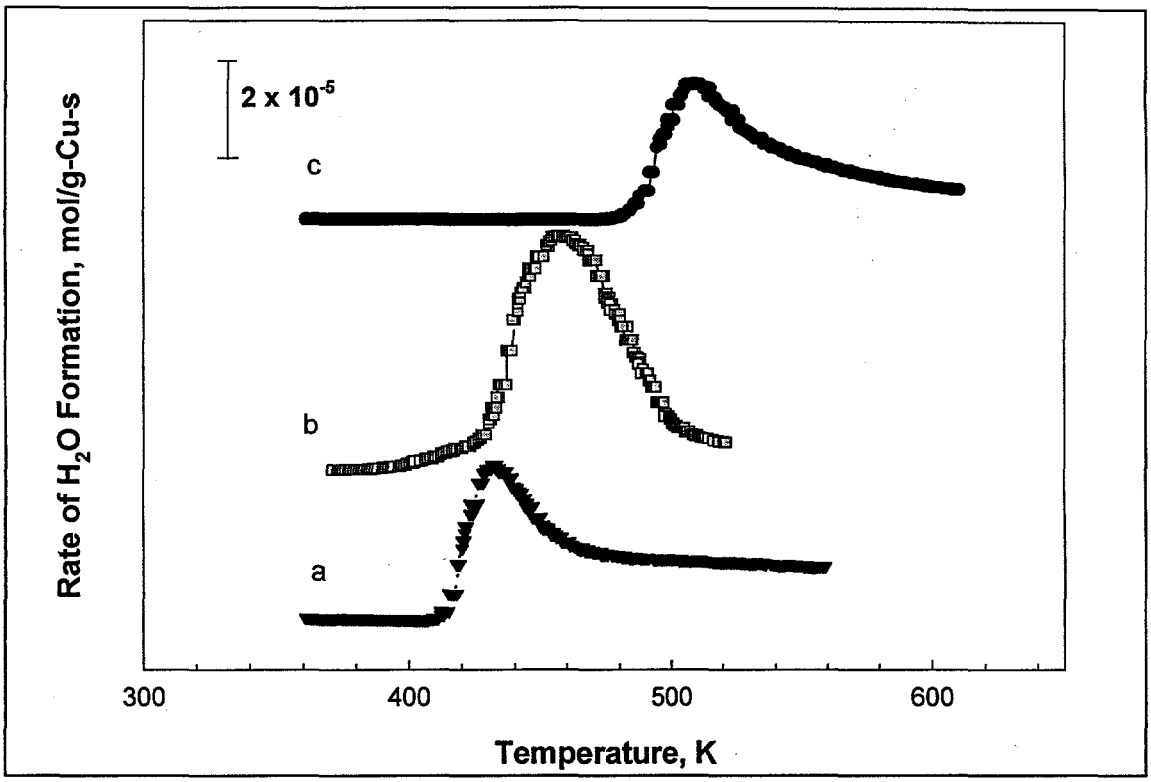

Figure 14. Temperature-programmed reduction profiles obtained in 5 % H_2/He of MgO-based Cu catalysts: (a) $Cu_{0.5}Mg_5CeO_x$; (b) $Cu_{7.5}Mg_5CeO_x$; (c) $Cu_{0.1}Mg_5O_x$. [Heating rate: 0.17 K/s; 15-100 mg of sample, 100 cm^3/min 5% H_2/He mixture; pretreatment temperature: 723 K]

ZnO has an effect similar to that of CeO_x on copper reduction. Garcia-Fierro *et al.* (14, 16) reported that the fraction of copper oxide strongly interacting with ZnO increases with increasing Zn/Cu ratio and that such copper oxide species showed the highest reducibility. A kinetic model of reduction kinetics of CuO/ZnO suggests that the promoting effect of ZnO on copper reduction is caused by the dissociative adsorption of H_2 on ZnO surfaces or on Cu metal clusters closely associated with ZnO (17). The spillover of the hydrogen atoms formed increases the rate of Cu^{2+} reduction. In fact, kinetic analysis showed that the apparent activation energy, E_a, was 84 kJ/mol for the reduction of pure CuO whereas E_a decreased to 77 kJ/mol for the reduction of the CuO-ZnO catalysts (14), in agreement with the promoting effect of ZnO on the reducibility of CuO. Similar processes are likely to occur during CuO reduction on $CuMgCeO_x$ samples. A better contact between CeO_x and Cu is expected with increasing CeO_x/Cu ratio, leading to CuO reduction at lower temperatures.

In contrast to CeO_x, K addition to Cu-containing samples inhibits CuO reduction, as shown by the shift of the reduction peak to higher temperatures (Figure 15). The effect of K is more pronounced on low-Cu ($Cu_{0.5}Mg_5CeO_x$) than on high-Cu ($Cu_{7.5}Mg_5CeO_x$) catalysts (ΔT = 79 K on the former compared to 57 K on the latter). Also, the effect of K was not influenced by the presence of CeO_x; the reduction temperatures increased by approximately the same amount (ΔT = 70 K) on K-$Cu_{0.5}Mg_5O_x$ and K-$Cu_{0.5}Mg_5CeO_x$. K appears to increase the stability of Cu^{2+} ions and make them more difficult to reduce by H_2. A similar effect has been reported on Cs-promoted $Cu/ZnO/Cr_2O_3$ (12). In this study, the presence of Cs retards CuO reduction by about

50 K. Klier and co-workers [12] suggest that the inhibited reduction of CuO is associated to closer interaction between the CuO and promoter phases which inhibited to some extent H_2 activation.

The inhibition effect of K on copper reduction observed in this study can be explained by the inhibited activation of H_2 proposed by Klier and co-workers (12) or by the strengthening of Cu-O bonds upon K addition. As reported in the literature (18, 19), the bond energy of surface oxygen for CuO is about 42 kJ/mol and it increases to 63 kJ/mol upon the addition of 10-25 at. % MgO. Addition of MgO weakens the Cu-Cu bonds and strengthens Cu-O bonds. In a similar way, the incorporation of K_2O into CuO during catalyst synthesis may increase the bond strength of Cu-O and therefore retard CuO reduction.

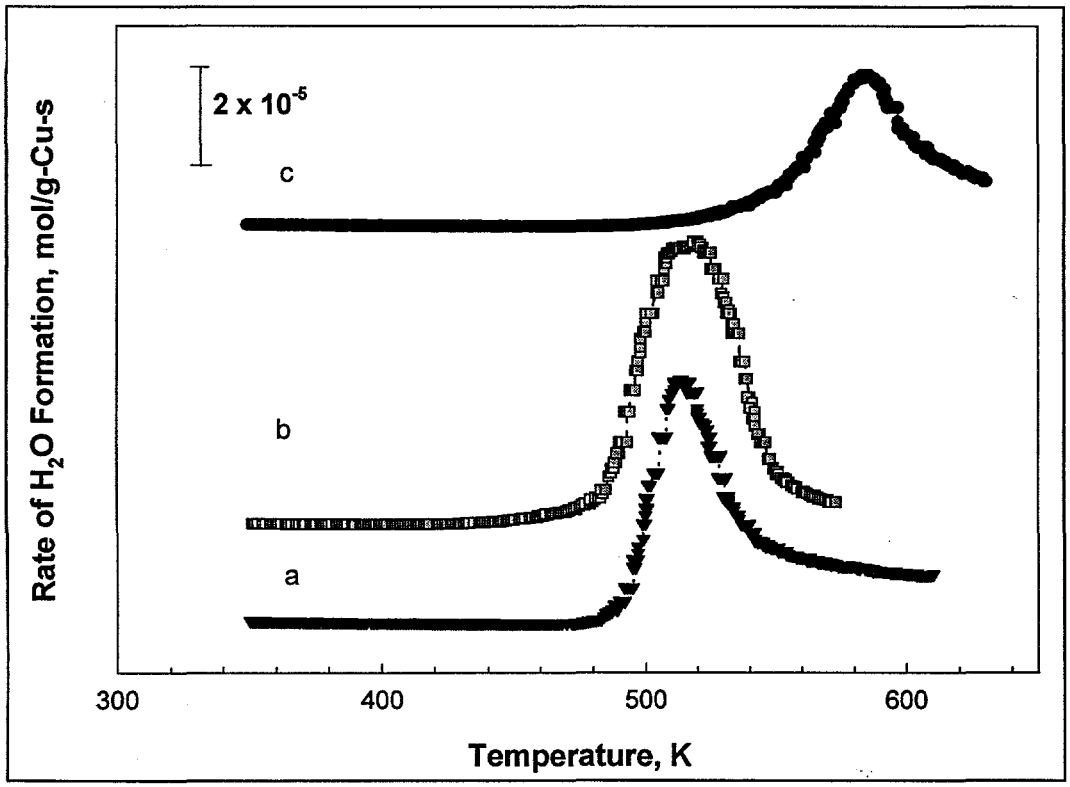

Figure 15. Temperature-programmed reduction profiles obtained in 5 % H_2/He of MgO-based Cu catalysts: (a) 1.0 wt % K-$Cu_{0.5}Mg_5CeO_x$; (b) 1.2 wt % K-$Cu_{7.5}Mg_5CeO_x$; (c) 1.1 wt % K-$Cu_{0.1}Mg_5O_x$. [Heating rate: 0.17 K/s; 15-100 mg of sample, 100 cm^3/min 5% H_2/He mixture; pretreatment temperature: 723 K]

4.2. Determination of Copper Surface Area

The decomposition of N_2O was used to measure Cu surface area of MgO-based Cu Catalysts. In a typical experiment, the catalyst was first reduced at 623 K in flowing H_2 (5 % H_2/He). After reduction, the reactor temperature was lowered to 363 K in flowing He and N_2O decomposition was then conducted via N_2O pulse injections. The Cu surface area was 28.5 m^2/g-cat (Cu dispersion: 6.8 %) for $CuZnAlO_x$ and 23.5 m^2/g (Cu dispersion: 5.2 %) for Cs-

$CuZnAlO_x$, suggesting the addition of Cs to $CuZnAlO_x$ decreases the number of surface exposed Cu atoms. The decrease in Cu surface area upon Cs addition could be due to a decrease in total surface area (from 74 to 62 m^2/g) and blocking of surface Cu by Cs_2CO_3.

The Cu surface area was found to be 13.1 m^2/g-cat (Cu dispersion: 15.8 %) on 1.0 wt % K-$Cu_{0.5}Mg_5CeO_x$ (MG3-13 o/K). The 15.8 % of Cu dispersion on MG3-13 o/K is comparable with the value of 14.1 % obtained on MG-11 ow/K (1.0 wt % K-$Cu_{0.5}Mg_5CeO_x$), suggesting the reproducibility in catalyst preparation. MG3-13 o/K and MG3-11 o/K have the same catalytic compositions but are prepared at different time.

In a typical CMRU experiment, the catalyst deactivates with time on stream. Cu surface area of the used sample (1.0 wt % K-$Cu_{0.5}Mg_5CeO_x$) was determined in order to address the effect of high-pressure catalytic reactions on Cu surface area. The used sample was first treated in flowing He at 723 K for 20 min followed by H_2 reduction at 623 K for 30 min before N_2O titration commenced at 363 K. The copper dispersions on the used 1.1 wt % K-$Cu_{0.5}Mg_5CeO_x$ taken from the top and middle-bottom of the CMRU catalyst bed were 3.6 % and 1.2 %, respectively. The smaller value in the latter suggests that the front part of the catalyst bed in the CMRU reactor is less severely deactivated. It should be pointed out that the total surface areas of these two used samples are comparable. The Cu dispersion of the used sample, however, was much less than that of the fresh sample (15.8 %). The decrease in Cu during reaction is due to 1) a decrease in the total surface area (150 m^2/g to 80 m^2/g) 2) deposition of hydrogen deficient hydrocarbon species on the catalyst surface, and 3) Cu metal sintering during the reaction.

In another experiment, the used 1.0 wt % K-$Cu_{0.5}Mg_5CeO_x$ removed from the top of CMRU reactor was treated in flowing O_2 (5 % O_2/He) instead of He at 723 K. This treatment leads to a Cu dispersion of 20.6 % that is even greater than the fresh sample even though the total surface area of the used sample is still approximately one-half of the fresh sample, suggesting that oxygen treatment at 723 K is able to remove all the species covering on Cu metal atoms. Moreover, alcohol (ROH) and water formed during the reaction could react with surface K^+ ions to form RO^-K^+ and KOH. The loss of RO^-K^+ and water from surface to gas phase results in a loss of surface K^+ ions and an increase in the exposed surface Cu atoms.

4.3 *Determination of Basic Site Density and Strength*

The density of basic sites was determined using a $^{13}CO_2/^{12}CO_2$ exchange method developed as part of this project; this method provides a direct measure of the number of basic sites *"kinetically available" at reaction conditions*. In addition, this technique provides a measure of the distribution of reactivity for such basic sites. In this method, a pre-reducecd catalyst is exposed to a 0.1 % $^{13}CO_2$/0.1 % Ar/He stream and after $^{13}CO_2$ reached a constant level in the effluent, the flow is switched to 0.1 % $^{12}CO_2$/He 573 K. The relaxation of the $^{13}CO_2$ removed from the surface is followed by mass spectrometry and the result obtained on 1.0 wt % K-$Cu_{0.6}Mg_5Ce_{1.2}O_x$ catalyst (MG3-13 o/K) is shown in Figure 16. The presence of Ar permitted the correction for gas-phase holdup and hydrodynamic delays. The exchange capacity at 573 K is calculated from the areas of the $^{13}CO_2$ and Ar peaks. The number of available basic sites in MG3-13 o/K (1.0 wt % K-$Cu_{0.5}Mg_5CeO_x$) is 1.85 x 10^{-6} mol/m^2, which is comparable to the amount (2.33 x 10^{-6} mol/m^2) obtained on MG3-11 ow/K (1.0 wt % K-$Cu_{0.5}Mg_5CeO_x$). This

suggests the reproducibility in catalyst preparation. Weakly interacting sites are mostly unoccupied by CO_2 and strongly interacting sites do not exchange in the time scale of the isotopic relaxation experiment. Neither strongly interacting nor weakly interacting sites are likely to contribute to catalytic reactions at similar temperatures.

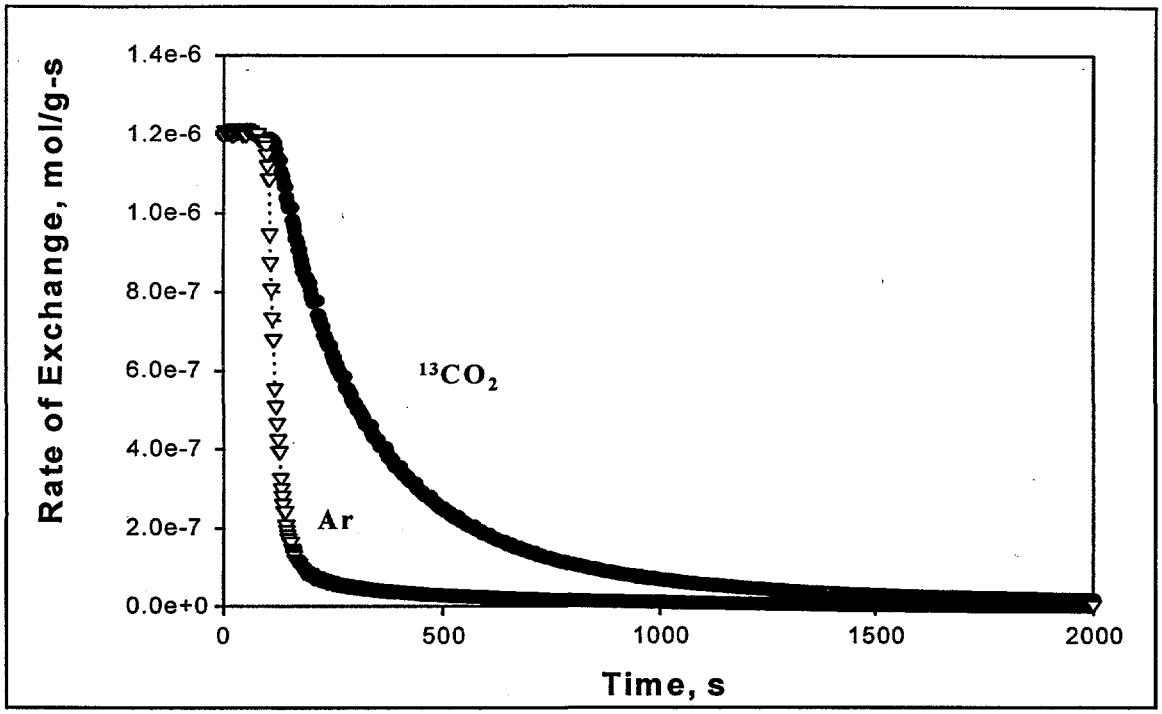

Figure 16. The transient response observed for 1.0 wt % K-$Cu_{0.6}Mg_5Ce_{1.2}O_x$ (MG3-13 o/K) upon switching from $^{13}CO_2$ to $^{12}CO_2$: T = 573 K.

In the experiment mentioned above, the number of available basic sites at 573 K was determined at a total gas flow rate of 100 cm^3/min with 50 mg catalyst charge. We explored the effect of carrier gas flow rate on shapes of the $^{13}CO_2$ transient curves in order to determine the significance of readsorption. In this experiment, three different flow rates (50, 100, and 200 cm^3/min) were used with the amount of catalyst (MG3-11 oW/K, 50 mg) remained unchanged. The number of available basic sites on 1.1 wt % K-$Cu_{0.5}Mg_5CeO_x$ (MG3-11 oW/K) at 573 K determined at these flow rates are comparable (1.8 ± 0.1 mol/m^2). The slopes of these curves, however, increases with increasing flow rates (Figure 7). As one can tell from the mathematical treatment (see Appendix), the gas phase concentrations of desorption products appear to depend on the rates of both desorption and carrier gas flow. The curve slope is a function of desorption rate constant (k_a), adsorption rate constants (k_d), and gas residence time (tr).

$$C_A(t)=C_{Ao}\cdot\frac{\frac{1}{\tau}-k_a}{\frac{1}{\tau}+k_a}-\frac{\theta_o}{\xi}\cdot\exp\left[\left(k_a-k_d+\frac{1}{\tau}\right)\cdot t\right]+\left[C_o-C_{Ao}\cdot\frac{\frac{1}{\tau}-k_a}{\frac{1}{\tau}+k_a}+\frac{\theta_o}{\xi}\right]\cdot\exp\left[-\left(\frac{1}{\tau}+k_a\right)\cdot t\right]$$

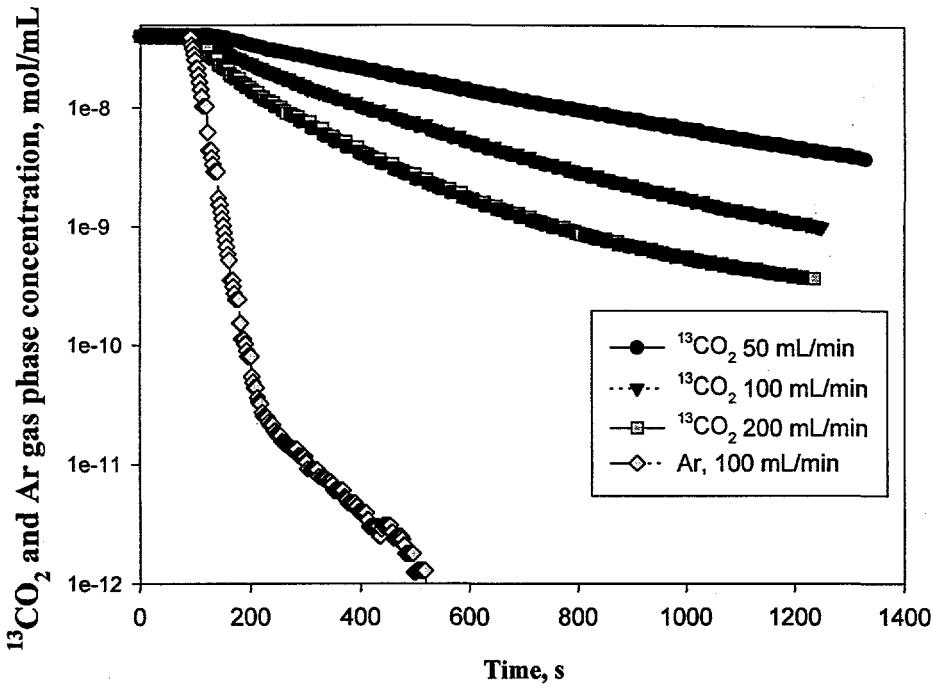

Figure 17. Effect of carrier gas flow rate on the shape of $^{13}CO_2$ transient curve on 1.1 wt% K-$Cu_{0.5}Mg_5CeO_x$ catalysts at 573 K.

Task 5: Bench Scale Testing at Air Products and Chemicals

Activities during this reporting period include meeting with Dr. Bernard A. Toseland from Air Products and Chemicals at Berkeley.

Staffing Plans

No changes.

Other activities

The manuscript *"Isobutanol and Methanol Synthesis on Copper Catalysts Supported on Modified Magnesium Oxide"* has been submitted to Journal of Catalysis for publication. A manuscript entitled *"Isotopic Switch Methods for the Characterization of Basic Sites in Modified MgO Catalysts"* is in the final draft and will be submitted for publication during the next reporting period.

Two abstracts *"Synthesis of Branched Alcohols on Bifunctional (Metal-Base) Catalysts Based on MgO Modified by CeO_x and Copper"* (M.J. Gines, M. Xu, A.M. Hilmen, B. Stephens, and E. Iglesia) and *"An Isotopic Swich Method for the Characterization of Basic Sites in Solids"* (M. Xu, Z. Hu, and E. Iglesia) were submitted to the 15th North American Meeting of the Catalysis Society.

A seminar (*"Reaction Pathways and Catalyst Requirements in the Synthesis of Isobutanol from CO and H_2 on K-CuMgCeO$_s$"*) was presented by Dr. M. Xu at the UOP Research Center.

References

1. Keim, W. and Falter, W., *Catal. Lett.* **3,** 59 (1989).
2. Dombeck, B.D., Heterogeneous Catalytic Process for Alcohol Fuels from Syngas, DOE Contract N° DE-AC 22-91PC90046, Final Technical Report, March 1996.
3. Elliot, D.J. and F. Penella, *J. Catal.* **119** (1989) 359.
4. Nunan, J.G., Bogdan, C.E., Klier, K., Smith, K., Young, C., and Herman, R., *J. Catal.* **116,** 195 (1989).
5. Klier, K., Chatikavanij, V., Herman, R.G., and Simmons, G.W., *J. Catal.,* **74,** 343 (1982).
6. Owen, G., Hawkes, C.R., Lloyd, D., Jennings, J.R., and Lambert, R.M., and Nix, R.M., *Appl. Catal.* **53,** 405 (1987).
7. Pan, W.X., Cao, R., Roberts, D.L., Griffin, G.L., J. Catal. 114 (1988) 440-446.
8. Hoppener, R.H., Doesburg, E.B.M., Scholten, J.J.F., App.Catal. (1986)109-119.
9. Chinchen,, G.C., Waugh, K.C., Whan, D.A., App. Catal. 25 (1986) 101-107.
10. Robbins, J.L., Iglesia, E., Kelkar, C.P., DeRites, B., Catal. Lett. 10 (1991) 1-10.
11. US patent 5,387,570.
12. Campos-Martin, J.M., Fierro, J.L.G., Guerrero-Ruiz, A., Herman, R.G., Klier, K., J. Catal. 163 (1996) 418-428.
13. Souza-Monteiro, R., Noronha, F.B., Dieguez, L.C., and Schmal, M., *Appl. Catal.* **131,** 89 (1995).
14. Garcia-Fierro, J.L., Lo Jacono, M., Inversi, M., Porta, P., Cioci, F., and Lavecchia, R., *Appl. Catal.* **137,** 327 (1996).
15. Lamonier, C., Bennani, A., Duysser, A., and Wrobel, G., *J. Chem. Soc., Faraday Trans.,* **92(1),** 131 (1996).
16. Garcia-Fierro, J.L., Lo Jacono, M., Inversi, M., Porta, P., Lavecchia, R., and Cioci, F., *J. Catal.* **148,** 709 (1994).
17. Annesini, M.C., Lavecchia, R., Marrelli, L., Lo Jacono, M., Campa, M.C., Garcia-Fierro, J.L., Moretti, G., and Porta, P., *Solid State Ionics.* **63-65,** 281 (1993).
18. Davydova, L.P., Boreskov, G.K., Popovskii, V.V., Yurieva, T.M., and Anufrienko, V.F., *React. Kinet. Catal. Lett.* **18,** 203 (1981).
19. Aleksandrov, V.Yu., Popovskii, V.V., and Bulgakov, N.N., *React. Kinet. Catal. Lett.* **8,** 65 (1978).

4. PARTICIPATING PROJECT PERSONNEL

Mingting Xu
Postdoctoral Fellow

Marcelo J. L. Gines
Postdoctoral Fellow

Anne-Mette Hilmen
Postdoctoral Fellow

Zhengjie Hu
Undergraduate Researcher

Bernard A. Toseland
Sub-Contractor
Air Products and Chemicals

Enrique Iglesia
Principal Investigator

Appendix

Mathematical treatment of relaxation profile of $^{13}CO_2$ from catalyst surface

Nomenclature:

N_A	Moles of $^{13}CO_2$	Wg	Weight of catalysts (g)
F_{Ao}	Inlet $^{13}CO_2$ molar flow rate (mol/s)	V	Reactor volume (cm^3)
F_A	Outlet $^{13}CO_2$ molar flow rate (mol/s)	S_A	Catalyst surface area (m^2/g)
C_A	Outlet $^{13}CO_2$ concentration (mol/cm^3)	rt	Residence time (s)
C_{Ao}	Inlet $^{13}CO_2$ concentration (mol/cm^3)	v	Volumetric flow rate (cm^3/s)
θ	$^{13}CO_2$ surface concentration (mol/m^2)	k_d	Desorption rate constant (s^{-1})
θ_0	$^{13}CO_2$ initial surface concentration (mol/m^2)	k_a	Readsorption rate constant (s^{-1})
C_0	Total gas phase concentration (mol/cm^3)		

From mass balance, we get:

$$\frac{dN_A}{dt} = \left(F_{Ao} - F_A\right) + k_d \cdot \theta \cdot S_A \cdot W_g - k_a \cdot C_A \cdot V$$

$$V \cdot \frac{dC_A}{dt} = \left(C_{Ao} \cdot v - C_A \cdot v\right) + k_d \cdot \theta \cdot S_A \cdot W_g - k_a \cdot C_A \cdot V$$

$$\frac{dC_A}{dt} = \frac{C_{Ao} - C_A}{\tau} + \frac{k_d \cdot \theta \cdot S_A \cdot W_g}{V} - k_a \cdot C_A$$

Two coupled differential equations to be solved are as follows:

$$\frac{dC_A}{dt} = \frac{C_{Ao} - C_A}{\tau} + k_d \cdot \theta \cdot S_A \cdot \frac{W_g}{V} - k_a \cdot C_A$$

$$\frac{d\theta}{dt} = \frac{k_a \cdot C_A \cdot V}{S_A \cdot W_g} - k_d \cdot \theta$$

Simplify the above equations:

$$\frac{dC_A}{dt} + \left(\frac{1}{\tau} + k_a\right) \cdot C_A - \frac{S_A \cdot W_g}{V} \cdot k_d \cdot \theta = \frac{C_{Ao}}{\tau}$$

$$\frac{d\theta}{dt} - \frac{V}{S_A \cdot W_g} \cdot k_a \cdot C_A + k_d \cdot \theta = 0$$

let $$\xi = \frac{V}{S_A \cdot W_g}$$

Plugging in:

$$\frac{dC_A}{dt} + \left(\frac{1}{\tau} + k_a\right)\cdot C_A - \frac{k_d}{\xi}\cdot\theta = \frac{C_{Ao}}{\tau}$$

$$\frac{d\theta}{dt} - \xi\cdot k_a \cdot C_A + k_d\cdot\theta = 0$$

Divide the second equation by εk_a

$$\left[D + \left(\frac{1}{\tau} + k_a\right)\right]\cdot C_A - \frac{k_d}{\xi}\cdot\theta = \frac{C_{Ao}}{\tau}$$

$$-C_A + \left(\frac{k_d + D}{\xi\cdot k_a}\right)\cdot\theta = 0$$

Do operation , $(D+1/\tau+k_d)$, on the 2nd equation and add it to the first equation to get a new 2nd equation:

$$\left[D + \left(\frac{1}{\tau} + k_a\right)\right]\cdot C_A - \frac{k_d}{\xi}\cdot\theta = \frac{C_{Ao}}{\tau} \qquad (1)$$

$$\left[\frac{-k_d}{\xi} + \left(\frac{k_d}{\xi\cdot k_a} + \frac{D}{\xi\cdot k_a}\right)\cdot\left[D + \left(\frac{1}{\tau} + k_a\right)\right]\right]\cdot\theta = \frac{C_{Ao}}{\tau} \qquad (2)$$

Now the 2nd equation is only in terms of θ only. It is just a second order nonhomogenuous differential equation. Simplifying (2) we get:

$$\left[D^2 + \left(k_d + k_a + \frac{1}{\tau}\right)\cdot D + \frac{k_d}{\tau}\right]\cdot\theta = \frac{C_{Ao}\cdot\xi\cdot k_a}{\tau}$$

or in other words:

$$\frac{d^2\cdot\theta}{dt^2} + \left(k_d + k_a + \frac{1}{\tau}\right)\cdot\frac{d\theta}{dt} + \frac{k_d}{\tau}\cdot\theta = \frac{C_{Ao}\cdot\xi\cdot k_a}{\tau} \qquad (3)$$

Equation (3) is a nonhomogenuous second order differential equation with constant coefficients. Its solutions are outlined in "Advanced Engineering Mathmetics" by Wylie and Barrett (see 5th edition, page 98)

$\theta(t)$ = complementary function + particular function.

The characteristic equation of (3) is:

$$m^2 + \left(k_d + k_a + \frac{1}{\tau}\right)\cdot m + \frac{k_d}{\tau} = 0$$

Solution to the above characteristic equation is:

$$m_1 = \frac{-\left(k_d + k_a + \frac{1}{\tau}\right) + \sqrt{\left(k_d + k_a + \frac{1}{\tau}\right)^2 - \frac{4\cdot k_d}{\tau}}}{2}$$

$$m_2 = \frac{-\left(k_d + k_a + \frac{1}{\tau}\right) - \sqrt{\left(k_d + k_a + \frac{1}{\tau}\right)^2 - \frac{4\cdot k_d}{\tau}}}{2}$$

Assume: $\left(k_d + k_a + \frac{1}{\tau}\right)^2 \geq \frac{4\cdot k_d}{\tau}$

So: $m_1 = 0$

$$m_2 = -k_d - k_a - \frac{1}{\tau}$$

Therefore the complementary function is as follows where m_1 and m_2 are expressed above:

$$c_1 + c_2\cdot\exp\left(m_2\cdot t\right)$$

Next step is to find particular integral to complete the solution.

Assumeθ=At^2+Bt+C therefore:

$$\frac{d\theta}{dt}=2At+B$$

$$\frac{d^2\cdot\theta}{dt^2}=2A$$

Plugging into equation (3):

$$2A+\left(k_d+k_a+\frac{1}{\tau}\right)\cdot(2At+B)+\frac{k_d}{\tau}\cdot(At^2+Bt+C)=\frac{C_{Ao}\cdot\xi\cdot k_a}{\tau}$$

From above we can get the following eqations:

$$\frac{k_d}{\tau}\cdot A=0$$

$$\left(k_d+k_a+\frac{1}{\tau}\right)\cdot 2A+\frac{k_d\cdot B}{\tau}=0$$

$$2A+\left(k_d+k_a+\frac{1}{\tau}\right)\cdot B+\frac{k_d\cdot C}{\tau}=\frac{C_{Ao}\cdot\xi\cdot k_a}{\tau}$$

Solve these 3 equtions, we get:

$$A=0$$

$$B=0$$

$$C=\frac{C_{Ao}\cdot\xi\cdot k_a}{k_d}$$

Therefore a particular solution is:

$$\theta=\frac{C_{Ao}\cdot\xi\cdot k_a}{k_d}$$

Therefore the general solutions is thus:

$$\theta=\frac{C_{Ao}\cdot\xi\cdot k_a}{k_d}+c_1+c_2\cdot\exp\left(m_2\cdot t\right) \qquad (4)$$

where c_1 and c_2 are two constants determined by boundary conditions.
The boundary conditions are as follows:

$\theta=\theta_o$ at $t=0$

$\theta=0$ at $t=\infty$

Plugging boundary conditions into (4), we can solve for C_1 and C_2:

$$c_1=\frac{-C_{Ao}\cdot\xi\cdot k_a}{k_d}$$

$$c_2=\theta_o$$

Therefore,$\theta(t)$ is:

$$\theta(t)=\frac{-C_{Ao}\cdot\xi\cdot k_a}{k_d}+\theta_o\cdot\exp\left[-\left(k_d+k_a+\frac{1}{\tau}\right)\cdot t\right] \qquad (5)$$

We need to get a similar expression for C_A. Now plugging equation 4 to equation 1:

$$\frac{dC_A}{dt}+\left(\frac{1}{\tau}+k_a\right)\cdot C_A=\frac{k_d\cdot\theta_o}{\xi}\cdot\exp\left[-\left(k_d+k_a+\frac{1}{\tau}\right)\cdot t\right]+\frac{C_{Ao}}{\tau}-C_{Ao}\cdot k_a \qquad (6)$$

Integrating factor for the above differential equation is :

$$\mu(t)=\exp\left[\left(\frac{1}{\tau}+k_a\right)\cdot t\right]$$

The general solution is as following, where C is a constant:

$$C_A(t)=\mu(t)^{(-1)}\cdot\left[\int \mu(t)\cdot\left[\frac{k_d\cdot\theta_o}{\xi}\cdot\exp\left[-\left(k_d+k_a+\frac{1}{\tau}\right)\cdot t\right]+\frac{C_{Ao}}{\tau}-C_{Ao}\cdot k_a\right]dt+C\right]$$

Solve it and we get:

$$C_A(t)=C_{Ao}\cdot\frac{\frac{1}{\tau}-k_a}{\frac{1}{\tau}+k_a}-\frac{\theta_o}{\xi}\cdot\exp\left[\left(k_a-k_d+\frac{1}{\tau}\right)\cdot t\right]+C\cdot\exp\left[-\left(\frac{1}{\tau}+k_a\right)\cdot t\right]$$

Plugging the boundary condition, $C_A = C_0$ at $t = 0$

$$C_o = C_{Ao} \cdot \frac{\frac{1}{\tau} - k_a}{\frac{1}{\tau} + k_a} - \frac{\theta_o}{\xi} + C$$

Therefore the complete solution is:

$$C_A(t) = C_{Ao} \cdot \frac{\frac{1}{\tau} - k_a}{\frac{1}{\tau} + k_a} - \frac{\theta_o}{\xi} \cdot \exp\left[\left(k_a - k_d + \frac{1}{\tau}\right) \cdot t\right] + \left[C_o - C_{Ao} \cdot \frac{\frac{1}{\tau} - k_a}{\frac{1}{\tau} + k_a} + \frac{\theta_o}{\xi}\right] \cdot \exp\left[-\left(\frac{1}{\tau} + k_a\right) \cdot t\right] \quad (7)$$

DOE F 1332.3
(11-84)

U.S. DEPARTMENT OF ENERGY
MILESTONE SCHEDULE ☐ PLAN ☒ REPORT

FORM APPROVED
OMB 1901-1400

1. TITLE	2. REPORTING PERIOD	3. IDENTIFICATION NUMBER
ISOBUTANOL METHANOL MIXTURE FROM SYNGAS	Oct. 1, 1996 - Dec. 31, 1996	DE - AC22 - PC94PC066

4. PARTICIPANT NAME AND ADDRESS	5. START DATE	6. COMPLETION DATE
Department of Chemical Engineering University of California - Berkeley	Oct 1994	Sept 1997

7. ELEMENT CODE	8. REPORTING ELEMENT	9. DURATION 94 ← 95 → ← 96 → ← 97 → Q1 Q2 Q3 Q4 Q1 Q2 Q3 J A S O N D J F M A M J J A S	10. PERCENT COMPLETE a Plan	b Actual
	Task 4	Identify reaction intermediates by TPSR and high pressure infrared methods	75	75
	Tasks 3 & 5	Identify catalysts with highest isoalcohol yields (two) and evaluate at conditions resembling envisioned commercial practice.	80	80
	Task 5	Assess economic viability of these catalytic materials	65	NA
	Task 5	Complete testing of at least two selected catalysts in slurry reactors.	65	0
	Tasks 3 & 5	Choose two materials for detailed studies of the reaction mechanism and of optimum synthetic protocols	50	50
	Tasks 3 & 5	Complete mechanistic studies on most promising materials	0	0
	Tasks 2 & 5	Develop synthetic procedures that can be carried out on a commercial scale Suggest a range of catalyst compositions for future study.	0	0
	Task 5	Complete testing of the two selected catalytic materials	0	0
	Task 5	Assess future research requirements, technical readiness and economic viability of the most promising approach	0	0
		Produce final report	0	0

DOE F 1332.3
(11-84)

U.S. DEPARTMENT OF ENERGY
MILESTONE SCHEDULE ☐ PLAN ☒ REPORT

FORM APPROVED
OMB 1901-1400

1. TITLE	2. REPORTING PERIOD	3. IDENTIFICATION NUMBER
ISOBUTANOL METHANOL MIXTURE FROM SYNGAS	Oct. 1, 1996 - Dec. 31, 1996	DE - AC22 - PC94PC066

4. PARTICIPANT NAME AND ADDRESS	5. START DATE	6. COMPLETION DATE
Department of Chemical Engineering University of California - Berkeley	Oct 1994	Sept 1997

7. ELEMENT CODE	8. REPORTING ELEMENT	9. DURATION	10. PERCENT COMPLETE a Plan	b Actual
	Task 3	Complete design, construction and start-up of packed bed reactor module	100	100
	Task 2	Prepare Cu-based catalyst compositions and characterize structure, surface area, and effectiveness of several synthetic approaches	100	100
	Task 2	Choose four promising materials for catalyst evaluation	100	100
	Task 3	Construct recirculating reactor module Establish reaction pathways and rate-determining steps	100	100
	Tasks 2 & 3	Identify catalyst components necessary to catalyze rate-determing steps that have been determined	100	100
	Tasks 2 & 3	Identify synthetic techniques to increase the reactivity and accessibility of such required sites	100	100
	Task 4	Complete construction and start-up of temperature programmed surface reaction apparatus and design of high-pressure infrared cell	100	100
	Task 4	Design and construction of high-pressure infrared cell	100	100
	Task 4	Calibrate between UCB and APCI laboratories by testing two selected catalysts	100	100
	Task 2	Determine the density and reactivity of the required sites and implement synthetic methods to improve them	80	75

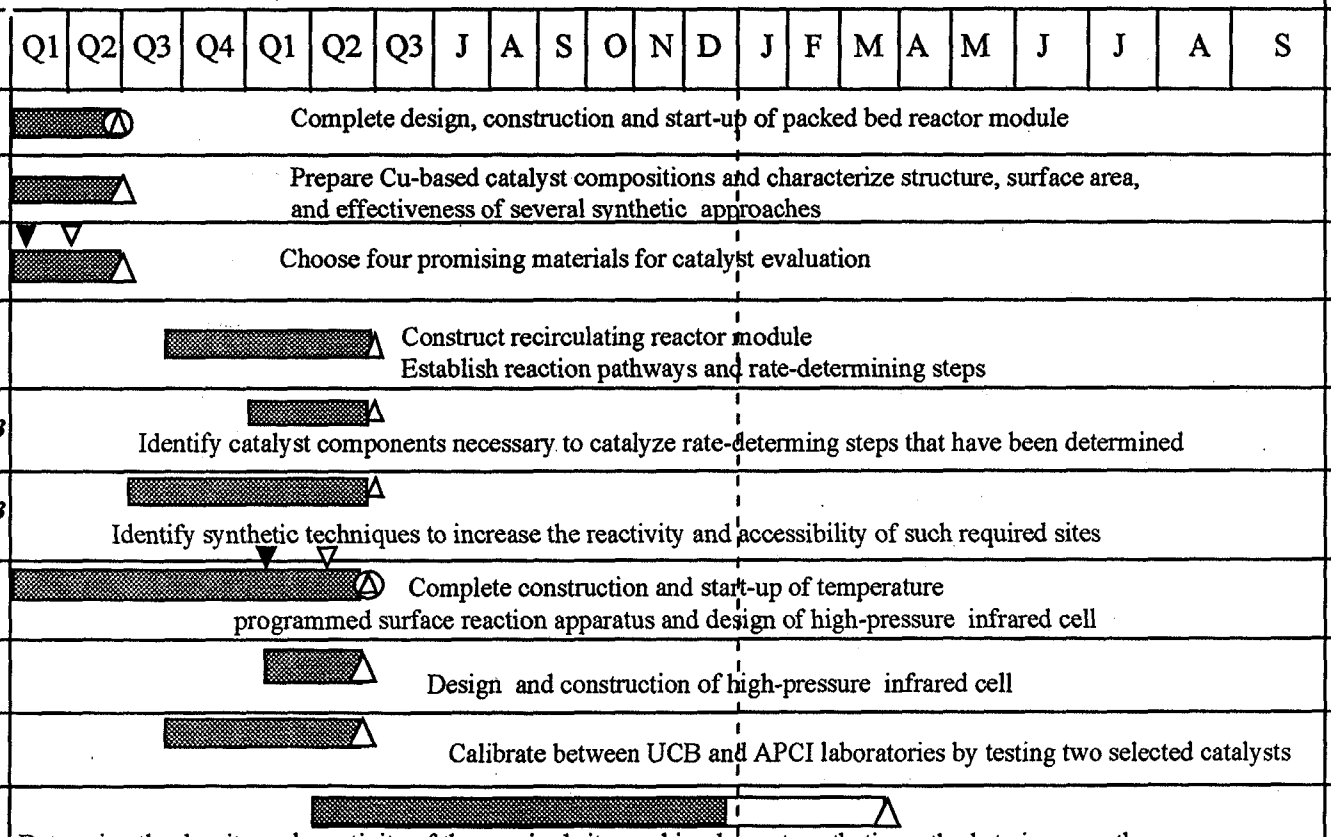

1. TITLE ISOBUTANOL- METHANOL MIXTURE FROM SYNGAS					2. REPORTING PERIOD October 1, 1996 to Dec. 31, 1996						3. IDENTIFICATION NUMBER DE-AC22-PC94PC066		
2. PARTICIPANT NAME AND ADDRESS Department of Chemical Engineering University of California- Berkeley, Berkeley, CA 94720					5. COST PLAN DATE Jan. 27, 1997						6. START DATE OCT 1994 7. COMPLETION DATE OCT 1997		
8. Element code	9. Reporting element	ACCRUED COSTS				ESTIMATED ACCRUED COSTS						12. Total contract Value	13. Variance
		Reporting period		Cumulative to date		a.total this fiscal year	b. balance of fiscal year	c. FY96 (1)	d. FY 97 (2)	(3)	e. total		
		a. Actual	b. Plan	c. Actual	d. Plan								
	1. Total (Direct material)	10,955	22,777	86,940	165,152	10,955	80,154	91,109	94,782		261,876	259,929	-1,947
	a) Purchased Parts	10,955	9,106	77,039	110,468	10,955	25,470	36,425	40,200		142,709	98,175	-44,534
	b) Subcontracted Items	0	13,670	3,970	128,722	0	54,679	54,679	54,582		113,231	161,754	48,523
	c) Other	0	0	5,931	74,043	0	0	0	0		5,931	0	-5,931
	2. Material Overhead	0	0	0	0	0	0	0	0		0	0	0
	3. Direct Labor 'Total	10,951	20,892	128,611	163,921	10,951	72,618	83,569	92,812		294,041	256,725	-37,316
	4. Labor Overhead	0	0	0	0	0	0	0	0		0	0	0
	5. Fringe Benefits	866	3,350	14,787	26,168	866	12,534	13,400	15,368		42,689	41,538	-1,151
	6. Special Testing	88	0	2,799	0	88	0	0	0		2,799	0	-2,799
	7. Special Equipment	0	2,000	290,137	260,000	0	8,000	8,000	0		298,137	260,000	-38,137
	8. Travel	421	1,629	7,339	12,720	421	6,094	6,515	7,020		20,453	19,740	-713
	9. Consultants	0	0	0	0	0	0	0	0		0	0	0
	10. Other Direct costs	0	6,114	0	47,745	0	24,455	24,455	25,677		50,132	73,422	23,290
	11. Direct costs and Overhead	23,280	56,761	530,613	675,702	23,280	203,764	227,044	235,653		970,030	911,354	-58,676
	12. General and Administrative Expense '49.5 %	11,617	20,505	119,886	165,757	11,617	70,403	82,020	90,358		280,646	256,108	-24,538
	13. Facilities Capital Cost of Money	0	0	0	0	0	0	0	0		0	0	0
	14. Total Estimated Cost	34,897	77,266	650,499	841,457	34,897	274,165	309,062	326,008		1,250,672	1,167,462	-83,210
	15. Fee	0	0	0	0	0	0	0	0		0	0	0
	16. Cost Sharing	0	9,949	205,766	252,851	0	39,797	39,797	56,789		302,352	301,651	-701
	17. Total estimated DOE funds spent = Item 14-Item 16	34,897	67,316	444,733	588,606	34,897	234,368	269,265	269,219		948,320	865,811	-82,509
14. Total		34,897	67,316	444,733	588,606	34,897	234,368	269,265	269,219		948,320	865,811	-82,509

15. DOLLARS EXPRESSED IN One U.S. Dollar	16. SIGNATURE OF PARTICIPANT PROJECT MANAGER AND DATE	17. SIGNATURE OF PARTICIPANT'S AUTHORIZED FINANCIAL SERVICE REPRESENTATIVE AND DATE Lourdes S. Farrer 1/27/97